Geometrical investigation of bluff bodies array subjected to forced convective flows for different aspect ratios of frontal body

# GEOMETRICAL INVESTIGATION OF BLUFF BODIES ARRAY SUBJECTED TO FORCED CONVECTIVE FLOWS FOR DIFFERENT ASPECT RATIOS OF FRONTAL BODY

F. B. Teixeira[1], C. Biserni[2,*], P. V. Conde[3], L. A. O. Rocha[4], L. A. Isoldi[3], and E. D. dos Santos[3]

[1]Mechanical Engineering Graduate Program, Universidade Federal do Rio Grande do Sul, Sarmento Leite st. 425, Porto Alegre, 90050-170 Brazil.

[2]Department of Industrial Engineering, Alma Mater Studiorum, University of Bologna, Viale Risorgimento 2, 40136 Bologna, Italy.

[3]School of Engineering, Universidade Federal do Rio Grande - FURG, Rio Grande, RS, Italia Avenue, km 8, 96201-900 Brazil.

[4]Mechanical Engineering Graduate Program, Universidade do Vale do Rio dos Sinos – UNISINOS, São Leopoldo, RS, Brazil.

*corresponding author: cesare.biserni@unibo.it

## Abstract

The present computational study comprises the geometrical investigation using the Constructal Design of a triangular array of bluff bodies subjected to incompressible, transient, and forced convective flows in a two-dimensional domain. It is considered a Reynolds and Prandtl numbers of $Re_D$ = 100 and $Pr$ = 0.71. The body areas and the maximum occupation area of the array are the problem constraints. The problem has three degrees of freedom (DOF): $S_T/D$, $S_L/D$ (ratios between transverse and longitudinal pitch over characteristic dimension $D$, respectively), and $H_1/L_1$ (height and length ratio of the upstream body of the arrangement). The objectives are to minimize the drag coefficient ($\overline{C_D}$) and maximization of heat transfer rate per unit length ($\bar{q}'$) of the arrangement. Conservation equations of mass, momentum, and energy are solved with the Finite Volume Method (FVM). Results indicated a significant gain in the fluid dynamic and thermal performances of 68.85% and 100.34%, respectively when the best and worst shapes are compared. Moreover, variations of the ratio $H_1/L_1$ strongly affected the behavior of $\overline{C_D}$ and $\bar{q}'$ as a function of $S_T/D$ and $S_L/D$ and optimal designs. Thermal streams with complex vortex structures distributed in tree-shaped patterns led to the highest heat transfer rate magnitudes.

**Keywords:** Forced Convection, Frontal Body Configuration, Constructal Design, Drag Coefficient, Heat transfer rate.

**NOMENCLATURE**

| | |
|---|---|
| $A$ | Area [m²] |
| $A_b$ | Cross-sectional area of bluff body [m²] |
| $A_t$ | Total area of bluff bodies in the arrangement [m²] |
| $C_D$ | Drag coefficient in the array ($C_D = 2F_D/(\rho V_\infty^2 A)$) [-] |
| $c_p$ | Specific heat of the fluid [J/(kg·K)] |
| $D$ | Dimension of square bluff bodies [m] |
| $F_D$ | Drag force [N] |
| $H$ | Convection heat transfer coefficient [W/(m²·K)] |
| $H$ | Height of channel where the array is inserted [m] |
| $H_0$ | Height of occupation area where the bodies are inserted [m] |
| $H_1$ | Height of upstream bluff body [m] |
| $k$ | Thermal conductivity of the fluid [W/(m·K)] |
| $L$ | Length of the channel where the array is inserted [m] |
| $L_0$ | Length of occupation area where the bodies are inserted [m] |
| $L_1$ | Length of upstream bluff body [m] |
| $Nu_D$ | Nusselt number of square bluff body ($Nu_D = h \cdot D/k$) [-] |
| $P$ | Pressure [N/m$^2$] |
| $Pr$ | Prandtl number ($Pr = c_p \mu/k$) [-] |
| $q'$ | Heat transfer rate per unit length between the array and surrounding flow [W/m] |
| $Re_D$ | Reynolds number ($Re_D = \rho V_\infty D/\mu$) [-] |
| $S_L$ | Longitudinal pitch of triangular arrangement [m] |
| $S_T$ | Transverse pitch of triangular arrangement [m] |
| $T$ | Temperature [K] |
| $T_\infty$ | Temperature of the fresh stream [K] |

| | |
|---|---|
| $T_s$ | Temperature of the heated bodies [K] |
| $u$ | Fluid velocity in $x$-direction [m/s] |
| $v$ | Fluid velocity in $y$-direction [m/s] |
| $V_\infty$ | Velocity at the inlet of domain [m/s] |

**Greek symbols**

| | |
|---|---|
| $\alpha$ | Thermal diffusivity [$m^2 \cdot s^{-1}$] |
| $\mu$ | Dynamic viscosity of the fluid [kg/(m·s)] |
| $\upsilon$ | Kinematic viscosity of the fluid [$m^2/s$] |
| $\rho$ | Density of the fluid [$kg/m^3$] |

**Subscripts**

| | |
|---|---|
| F | Fluid |
| m | Once minimized or maximized |
| 2m | Twice minimized or maximized |
| 3m | Three times minimized or maximized |
| o | Once optimized |
| 2o | Twice optimized |
| 3o | Three times optimized |
| T | Thermal |

## 1. INTRODUCTION

Prediction of convective flows over obstacle arrangements has an increasing interest. Many applications can explain this interest where these arrangements are found: bulkheads, tube clusters, marine cables, urban structures, electronic packaging, and heat exchangers. In these systems, achieving the highest performance at the lowest cost and

volume occupation is always desirable. Therefore, the investigation of design in this kind of problem is also an important and challenging subject [1 – 3].

A series of works concerned with investigating internal and external flows over cylinders, bluff bodies, or blocks have focused on this premise. For instance, the study by Dulhani et al. [4] investigated the influence of the flow incidence angle on a square obstacle with mixed convection heat transfer. It was varied the Richardson number between $-1.0 \leq Ri \leq 1.0$ and the incidence angles in the range $0^o \leq \alpha_i \leq 45^o$, keeping Reynolds and Prandtl numbers fixed at 100 and 0.71, respectively. Effects of geometric variations in drag and lift coefficients ($C_D$ and $C_L$) were also studied.

Shadlaghani et al. [5] carried out a triangular and rectangular fins optimization study with and without longitudinal perforation. The objective was to optimize the fin with triangular configuration since the numerical results demonstrated its superior performance compared to the rectangular section fins. Other works investigated the influence of geometry on different obstacle shapes for isothermal and convective flows, such as elliptical cylinders [6, 7], square bodies [8], trapezoidal bodies [9], rectangular bodies [3, 10], cylinders with inserted radial fins [11], cylinders with protrusions [12], semi-circular cylinders [13], yawed cylinder [14] and even balloon-shaped bodies [15]. Recently, Pawar et al. [16] performed a numerical investigation of forced convective flows over a bluff body for different Reynolds numbers ($40 \leq Re \leq 160$) and incidence angle of the mainstream with the body ($0^o \leq \alpha \leq 160$). The blunt-headed cylinder led to a heat transfer rate higher than that reached for a similar rectangular shape. These studies illustrated that the investigation of one cylinder or obstacle with varied shapes subject to isothermal or convective flows still represents a significant problem.

The geometric evaluation of arrangement or pair of cylinders/bluff bodies under isothermal, forced, mixed, and natural convective flows has been the subject of various important recent studies. For instance, Gao et al. [17] investigated numerically three-dimensional isothermal flows over three cylinders equidistantly placed in a triangular arrangement. Different Reynolds numbers ($200 \leq Re \leq 3900$) and spacing ratios ($L/D$) were considered. It was noticed significant differences in the pressure coefficient for one of the downstream cylinders compared with the results for a single cylinder, independent of the values of $Re$ and $L/D$ investigated.

Pravesh et al. [18] investigated aiding buoyancy mixed convective flows across heated cylinders arranged in an aligned configuration. It was analyzed the influence of Reynolds ($1.0 \leq Re \leq 40.0$), Prandtl ($0.7 \leq Pr \leq 50.0$), and Richardson ($0.0 \leq Ri \leq 2.0$) for

different ratios between the total area of the fluid among the cylinders and the total area of the arrangement, named fluid volume fraction ($0.7 \leq \phi_f \leq 0.99$). Results indicated an increase of Nusselt number with the enhancement of Reynolds and Prandtl numbers, and the increase of fluid volume fractions for mixed convective flows, contrarily to observations found for flows dominated by forced convection ($Ri = 0.0$). Zhang et al. [19] studied forced convective flows over two bluff bodies arranged in tandem. The influence of curvature ratio was investigated for a square body ($R = 0.0D$), cylinder partially rounded ($R = 0.1D – 0.4D$) and circular one ($R = 0.5D$). The spacing between the cylinders was also investigated. The authors noticed that the cylinders' configuration affected the wake-flow behavior behind the downstream cylinder, being unsteady for square-shaped cylinders and stabilized for circular ones. Patel et al. [20] evaluated square cylinders arranged in the side-by-side configuration under mixed convective flows. It was investigated the influence of the Richardson number and incidence angle on the Nusselt number. Other examples of convective flows over pairs and cylinders' arrangements were presented in the literature [1 – 3, 21].

Despite several relevant studies, the study of bluff bodies arrangements with Constructal Design has been restricted to few investigations. Constructal Design is the method of application of Constructal Law, which is a physical principle that explains the generation and evolution of design in any flow system of finite size [22 – 27]. The application of Constructal Design is performed with the definition of the constraints (physical, geometrical, and others) and objectives (performance indicators). The geometry (degrees of freedom) is varied to improve the performance indicators.

Constructal Design has also been applied in some works to investigate convective flows over cylinders' arrangements and bluff bodies. Bello-Ochende and Bejan [28] studied arrangements of circular tubes with side-by-side configuration under natural convection heat transfer. The authors noticed that complex structures with small tubes between large cylinders increase heat transfer rate densities. Kim et al. [29] performed a computational study analyzing the influence of diameters size and distance between the system effectiveness tubes. It was considered a forced convection cross-flow in the arrangement's external side and natural convection into the tubes.

Bello-Ochende et al. [30] studied different sized rotational cylinders arrangement subject to forced convection flows, showing that the imposition of rotation can benefit the heat transfer for aligned configurations of the tubes. Afterward, Page et al. [31] studied the mounting of multi-scale rotating cylinders subject to natural convection heat transfer.

The authors investigated staggered configurations for the arrangement seeking the maximization of heat transfer rate. Recently, Barros et al. [32] analyzed numerically a triangular array of circular cylinders under mixed convection flows with varied Richardson numbers ($0.1 \leq Ri \leq 10.0$) for $Re_D = 100$ and $Pr = 0.71$. The goals are to minimize the drag coefficient and maximize the Nusselt number when two degrees of freedom (ratios between longitudinal and transverse pitches and the cylinder diameter) varied into an occupation area.

Concerning the study of geometric evaluation of rectangular cylinders arrangements, Teixeira et al. [33] evaluated the thermal and fluid-dynamic behaviors of a triangular array of square bluff bodies subject to turbulent flows with forced convection heat transfer. The design in turbulent flows is rarely optimized in the literature. The obstacles were placed in a computational domain, where the bluff bodies have fixed square shapes of unitary size *D*. The study has two degrees of freedom, being the ratios between the transverse and longitudinal pitches and their side dimension. Results showed that the multiplicity of scales that arises in turbulent flow is profoundly affected by square cylinders' arrangement. Moreover, fluid dynamic and thermal performance have substantial changes with design in the problem. Constructal Design associated with Exhaustive Search was also employed for geometrical investigation of similar problems, e.g., heated rectangular blocks mounted in a channel flow surface subject to forced and mixed convective flows [34, 35]. Other descriptive techniques have also been used to achieve interesting contributions about the design in convective heat transfer problems, as those found in treelike branching microchannels [36, 37].

In this way, the present work intends to use Constructal Design associated with Exhaustive Search to investigate the geometric configuration of a triangular array of bluff bodies subjected to forced convective flows for different height/length ratios frontal body. The ratio between height and width of the frontal body ($H_1/L_1$) changed on various ratios from 0.1 to 5.0, while the posterior bodies maintain a fixed square shape with edge *D*. Besides, for each ratio of $H_1/L_1$, the spacing $S_L/D$ and $S_T/D$ is varied as already described in [33], seeking to minimize the $\overline{C_D}$ and maximize $\bar{q}'$. The main novelty here is the investigation about how the frontal body's geometric configuration influences the effect of arrangement design over the fluid dynamic and thermal behaviors of forced convective flow and performance indicators of the system. At the best of the authors' knowledge, the consideration of different geometric configurations applying Constructal Design considering the variation of transversal and longitudinal pitches and the height/length

ratio of the frontal body was not investigated in the literature. The study is performed numerically with the aid of a Finite Volume Method CFD code, ANSYS Fluent, version 14.5 [38 – 40].

## 2. MATHEMATICAL MODELING AND GEOMETRIC INVESTIGATION

Here, it is presented the physical description of the studied problem, the application of Constructal Design for geometric evaluation, and the governing equations for each simulated case's solution.

### 2.1. Description of forced convective flow over bodies array

The present problem comprises an incompressible, laminar, transient forced convective flow in a two-dimensional channel. A triangular array of rectangular bluff bodies is inserted in the channel domain, as illustrated in Fig. 1. Moreover, the array presents the frontal body of variable geometric ratio ($H_1/L_1$) and the posterior bodies in the form of squares of size $D$. It is considered for all cases constant magnitudes of Reynolds and Prandtl numbers ($Re_D$ = 100 and $Pr$ = 0.71).

Since the problem consists of an external crossflow, edge $D$ is used as a characteristic dimension for calculating the Reynolds number, which coincides with the edge size of the posterior square-shaped bluff bodies. It is then imposed a velocity profile ($V_\infty$) on the entrance of the domain (left side of Fig. 1), so that $Re_D$ = 100. For the thermal exchange, all three bluff bodies are maintained at a surface temperature ($Ts = T_\infty + \Delta T$) where $\Delta T$ = 20 ºC. The forced convection heat transfer occurs due to the different temperatures for the flow and the obstacles. In the exit of the domain, it is considered a null thermal gradient and zero gauge pressure. Moreover, the symmetry boundary condition is imposed at the top and bottom faces. Figure 1 also depicts the domain dimensions. The parameter $S_T/D$ represents the ratio between the transverse pitch of downstream bluff bodies and the characteristic dimension $D$. Also, $S_L/D$ is the ratio of the longitudinal pitch between the upstream bluff body and the downstream bodies and the characteristic dimension $D$. The last degree of freedom is the $H_1/L_1$ ratio, representing the height and length ratio of the frontal bluff body.

In this work, $H_1/L_1$ is evaluated for five different values: $H_1/L_1$ = 0.1; 0.5; 1.0; 2.0 and 5.0. The $S_T/D$ and $S_L/D$ ratios are considered varying in the following values: 2.0 ≤

$S_T/D \leq 4.0$; $2.0 \leq S_L/D \leq 4.0$. A total of 125 simulations are performed to predict the recommendations for the best configurations which minimize the drag coefficient ($\overline{C_D}$) and lead to the highest heat transfer rates ($\bar{q}'$).

## 2.2. Constructal Design for geometric evaluation of the array

According to Bejan [27], the phenomenon of the evolution of freely morphing configuration in finite flow systems is a first principle named constructal law, being a thermodynamics principle as is the first and second law that represents the irreversibility and energy conservation phenomena.

The application and investigation of design in any finite flow system can employ the Constructal design method [23 – 24]. In this method, the flow system is subjected to constraints (geometrical, physical, and others), and the design evolves in such a way to facilitate the internal currents [25 – 26]. The performance indicators of the problem represent the ease of access to the internal currents. The main steps for applying the method on the problem are the definition of flow system (domain, boundary conditions), identification of performance indicators of the problem, definition of constraints, degrees of freedom, and the physical problem's main parameters to be investigated. Moreover, it is defined as the methodology used to predict the performance indicator for each studied geometry. It is worthy of mentioning that Constructal Design is a method for geometrical evaluation, defining the search space for analysis of different geometries. It is necessary for optimization to associate an optimization method (Exhaustive Search in the present work). A flowchart with a systematic explanation about the application of Constructal Design was presented in the recent work of Estrada et al. [41]. The steps used in that work are adapted for the present problem, and for the sake of brevity, the flowchart is not repeated here.

The geometric constraints defined with Constructal Design for this problem are defined as follows:

i) The three rectangular body' areas are the same and the bodies' total area is given by:

$$A_t = A_{b1} + A_{b2} + A_{b3} \tag{1}$$

ii) The occupation area of the simulation is defined as:

$$A_0 = H_0 \times L_0 = 25D^2 \tag{2}$$

iii) The channel domain dimensions are assumed as $H = 10D$ and $L = 50D$;

iv) The transverse pitch of downstream bluff bodies plus the size of bodies cannot exceed the height of the occupation area ($S_T + D \leq H_0$);

v) The height of the frontal body cannot exceed the height of the occupation area ($H_1 \leq H_0$);

vi) The total dimension of arrangement in a longitudinal direction cannot exceed the length of the occupational area ($L_1/2 + S_L/D + D/2 \leq L_0$);

vii) The obstacles cannot overlap with other bodies.

It is worthy of mentioning that the occupation area is not an area that circumscribes the arrangement, but a limit area which can be occupied by the arrangement in extreme configurations of the ratios $H_1/L_1$, $S_L/D$, and $S_T/D$. This occupation area is defined in such a way to limit the investigation search space of geometries, which simulates the displacement of the arrangement in a heat exchanger.

The problem has three degrees of freedom ($S_T/D$, $S_L/D$, and $H_1/L_1$) whose dimensions can be seen in Fig. 1.

The performance indicators investigated here are the time and space-averaged heat transfer rate per unit length ($\bar{q}'$) and drag coefficient ($\overline{C_D}$), which are given by:

$$\bar{q}' = \frac{\bar{h}_1 A_{s,1}(T_s - T_\infty)}{W} + \frac{\bar{h}_2 A_{s,2}(T_s - T_\infty)}{W} + \frac{\bar{h}_3 A_{s,3}(T_s - T_\infty)}{W} \tag{3}$$

$$\overline{C_D} = \frac{1}{3}\left(\frac{2F_{D,1}}{\rho V_\infty^2 A_1} + \frac{2F_{D,2}}{\rho V_\infty^2 A_2} + \frac{2F_{D,3}}{\rho V_\infty^2 A_3}\right) \tag{4}$$

where $T_s$ is the temperature in the surfaces of the bodies (K); $\bar{h}$ is the time and space-averaged convective heat transfer coefficient (W/(m$^2$.K)); $W$ is the three-dimensional dimension of the domain (m); $F_D$ is drag force (N). Concerning the areas used in the calculations, $A_s$ is the obstacle superficial area (m²) and $A$ is the transversal section area of the body (m$^2$) and subscript numbers 1, 2, and 3 are related with bodies 1, 2, and 3, respectively. The superficial areas used for prediction of heat transfer rate per unit length are given by: $A_{s,1} = 2(H_1 + L_1)W$, $A_{s,2} = A_{s,3} = 4DW$. The areas used in calculating the drag coefficient for the bodies are $A_1 = H_1W$ for the frontal body and $A_2 = A_3 = DW$ for the downstream areas. The $\overline{C_D}$ and $\bar{q}'$ magnitude for the arrangement is obtained by the arithmetic mean of these values obtained for the three bodies.

It is important to note that, since three degrees of freedom (DOF) are investigated, the optimization is performed in three stages. Figure 2 presents a flowchart with the main steps representing the application of Constructal Design and Exhaustive Search in the present problem. In the first stage, the geometry is optimized, changing the degree of freedom $S_T/D$, while the parameters $S_L/D$ and $H_1/L_1$ are fixed. The highest value found for the heat transfer rate per unit length ($\bar{q}'$) is called the once maximized heat transfer rate ($\bar{q}'_m$) and the geometry that leads to this highest value is named once thermally optimized $(S_T/D)_{o,T}$. A similar procedure is performed for the drag coefficient. However, the purpose is to minimize its magnitude. The lowest $\overline{C_D}$ obtained is the once minimized drag coefficient ($\overline{C_D}$,$_m$) with the geometry leading to this lower value being called once fluid dynamic optimized ratio $(S_T/D)_{o,F}$.

Afterward, the $S_L/D$ ratio is varied for different $S_T/D$ values, keeping only $H_1/L_1$ fixed. More precisely, the first step is done again for different magnitudes of $S_L/D$. The largest $\bar{q}'$ obtained is called the twice maximized heat transfer rate ($\bar{q}'_{2m}$), and the corresponding optimal configurations are the twice optimized ratio $(S_T/D)_{2o,T}$ and once optimized ratio $(S_L/D)_{o,T}$. A similar process is made to obtain the twice minimized drag coefficient ($\overline{C_D}$,$_{2m}$), as well as the twice optimized ratio $(S_T/D)_{2o,F}$, and once optimized ratio $(S_L/D)_{o,F}$ for fluid dynamic purpose.

Finally, in the third stage, $H_1/L_1$ is varied for different $S_T/D$ and $S_L/D$ values. The largest $\bar{q}'$ obtained is the three times maximized heat transfer rate ($\bar{q}'_{3m}$), and the corresponding optimal geometry is the three times optimized ratio $(S_T/D)_{3o,T}$, two times optimized ratio $(S_L/D)_{2o,T}$, and once optimized ratio $(H_1/L_1)_{o,T}$. A similar procedure is done to obtain the value of the drag coefficient minimized three times ($\overline{C_D}$,$_{3m}$), and the corresponding optimal geometry is the three times optimized ratio $(S_T/D)_{3o,F}$, two times optimized ratio $(S_L/D)_{2o,F}$ and once optimized ratio $(H_1/L_1)_{o,F}$.

## 2.3. Governing equations for each simulated case

With the geometric problem completely determined, the final question to address is the solution of the equations that govern the problem. For the laminar, incompressible, transient flows with forced convection heat transfer in two-dimensional domains, the modeling is represented by conservation equations of mass, momentum, and energy, written by [42]:

$$\frac{\partial u}{\partial x}+\frac{\partial v}{\partial y}=0 \tag{5}$$

$$\frac{\partial u}{\partial t}+u\frac{\partial u}{\partial x}+\upsilon\frac{\partial u}{\partial y}=-\frac{1}{\rho}\frac{\partial P}{\partial x}+\upsilon\left(\frac{\partial^2 u}{\partial x^2}+\frac{\partial^2 u}{\partial y^2}\right) \tag{6}$$

$$\frac{\partial v}{\partial t}+u\frac{\partial v}{\partial x}+\upsilon\frac{\partial v}{\partial y}=-\frac{1}{\rho}\frac{\partial P}{\partial y}+\upsilon\left(\frac{\partial^2 v}{\partial x^2}+\frac{\partial^2 v}{\partial y^2}\right) \tag{7}$$

$$\frac{\partial T}{\partial t}+u\frac{\partial \mathrm{T}}{\partial x}+v\frac{\partial \mathrm{T}}{\partial y}=\frac{k}{\rho c_p}\left(\frac{\partial^2 T}{\partial x^2}+\frac{\partial^2 T}{\partial y^2}\right) \tag{8}$$

where, $u$ and $v$ are respectively, the flow velocities in the $x$ and $y$ axis (m/s), $\rho$ is the density (kg/m$^3$), $\upsilon$ is the kinematic viscosity (m²/s), $t$ is the time (s), $P$ is the pressure (N/m$^2$), $T$ is the temperature (K), $k$ is the thermal conductivity of the fluid (W/(m.K)), and $c_p$ is the specific heat of the fluid (J/(kg.K)).

## 3. NUMERICAL MODELING

In this work, computational tools are used to carry out the numerical study. In the pre-processing, *Gmsh* software (version 4.5.0) is used to build the problem computational domain's geometry and generate the mesh. For the implementation of boundary conditions and processing the simulations, CFD ANSYS Fluent® 14.5 Finite Volume Method (FVM) code is used to solve Eqs. (5)-(8) [38 – 40].

For the simulation of transient cases, it is considered a time step of $\Delta t$ = 0.01 s. The solver is pressure-based, and the coupling between pressure and velocity is made with the SIMPLEC algorithm (*Semi-Implicit Method for Pressure-Linked Equations - Consistent*). The 2$^{nd}$ order upwind scheme is used to tackle with advective terms of momentum and energy equations. Moreover, the convergence is obtained for residuals of mass, momentum, and energy conservation equations lower than $10^{-6}$, $10^{-6}$, and $10^{-8}$, respectively, between two consecutive iterations. The total simulated time for each case is $t_f$ = 10.0 s, with a computational calculation time of about 15,000 s per case performed by a hexacore Intel Core i7 5820K running @ 3.3Ghz and a total of 16Gb of DDR4 2666Mhz RAM. It is observed that after $t$ = 5.0 s of simulated time, the thermal and fluid

dynamic behaviors begin to show repetitions in time, and the flow can be considered at a steady state. Therefore, the last 5.0 s of each simulation is considered for estimating time-averaged values of $C_D$ and $q'$.

To determine the meshes to be used, a study of mesh independence is performed, followed by a verification analysis of the computational model by comparing the present results and those presented in the literature.

The mesh acceptance criterion selected is given by:

$$\left|\frac{\overline{Nu_D^i} + \overline{Nu_D^{i+1}}}{\overline{Nu_D^i}}\right| < 1.0 \times 10^{-3} \tag{9}$$

where $Nu_D$ is the bluff bodies arrangement averaged Nusselt number for the investigated arrangement with $H_1/L_1 = 1.0$, $S_L/D = 2.0$ and $S_T/D = 4.0$, and "$i$" and "$i + 1$" are the tested mesh indexes.

Table 1 presents the variation of the Nusselt number as a function of the number of grid cells. All the studied cases use unstructured meshes of quadrilateral cells with approximately 50,000 volumes, as shown in Fig. 3. It is worth mentioning that there is a greater refinement of the mesh in the wall regions to capture the thermal and fluid dynamics gradients more appropriately. The same characteristics found for the independent grid are employed for the other geometrical configurations, mainly in the near walls where a higher refinement is required.

Table 1 – Mesh independence test for the arrangement of bluff bodies with $H_1/L_1 = 1.0$, $S_L/D = 2.0$ and $S_T/D = 4.0$.

| Mesh | Total number of cells | $\overline{Nu_D}$ | $\left\|\frac{\overline{Nu_D^i} + \overline{Nu_D^{i+1}}}{\overline{Nu_D^i}}\right\|$ |
|---|---|---|---|
| M1 | 8,304 | 4.3547 | - |
| M2 | 32,583 | 4.3908 | $8.27 \times 10^{-3}$ |
| M3 | 47,076 | 4.3829 | $1.78 \times 10^{-3}$ |
| **M4** | **50,394** | **4.3854** | $\mathbf{5.60 \times 10^{-4}}$ |

In addition to this test, numerical modeling results obtained here are carried out comparatively to several works of literature [43 – 51] to validate the present code. In a

first moment, it is verified the local Nusselt number with previous results of Sahu et al. [43] for an isolated cylinder and verification of the effect of $S_T/D$ over time and space-averaged Nusselt number for a triangular arrangement of bluff bodies, obtained by Teixeira et al. [44]. More precisely, Fig. 4 (a) shows the local Nusselt number for one obstacle using the current mesh construction and simulation procedures. It is observed that the results obtained agree with the existing literature with deviations not exceeding 2.3% on all surfaces of the obstacle. It is worth remembering that the values for $Re_D$ and $Pr$ here are slightly different from the values intended for this work, but they serve to verify the numerical model properly since the same flow conditions are investigated. In Fig. 4 (b), a comparison is seen for the average Nusselt number of the arrangement for several $S_T/D$ spacing with $S_L/D$ = 2.0 and $H_1/L_1$ = 1.0. In these cases, magnitudes of $Re_D$ = 100 and $Pr$ = 0.71 are used for verification. It is noted in the graph that the current modeling fully agrees with the results of the literature, showing deviations of the order of 1.0% only in the entire studied range and ensuring the suitability of the numerical model for geometric investigation proposed in this work.

In order to validate the present code, the drag coefficient and Nusselt number obtained for a square obstacle of dimension $D$ under forced convection flow with $Re_D$ = 100 and $Pr$ = 0.71 are compared with the results obtained with numerical and experimental results available in the literature [43, 45 - 51], as can be seen in Tab. 2. Results obtained with the present code are in close agreement with other numerical and experimental predictions of literature. It is worth mentioning that even different experimental results reported some differences, as can be seen in Norberg et al. [47] and Liu [50]. Therefore, the present code can be considered validated for posterior investigation of the geometry of the arrangement of bluff bodies.

Table 2 – Drag coefficient and Nusselt number for flows with $Re_D$ = 100 and $Pr$ = 0.71 over a square bluff body obtained in the present work and literature [43, 45 – 51].

| **Reference** | $C_D$ | **Relative Difference** | $Nu_D$ | **Relative Difference** |
|---|---|---|---|---|
| Present work | 1.4682 | -------- | 4.0166 | -------- |
| Sahu et al. [43] | 1.4878 | -1.31 % | 4.0254 | -0.22 % |
| Sharma and Eswaran [45] | 1.4936 | -1.70 % | 4.0439 | -0.68 % |
| Sohankar et al. [46] | 1.4640 | 0.29 % | -------- | -------- |

| | | | | |
|---|---|---|---|---|
| Norberg et al. [47] | 1.448 ± 0.025 | -1.40 % | -------- | -------- |
| Tanweer et al. [48] | -------- | -------- | 4.0250 | -0.21 % |
| Turki et al. [49] | -------- | -------- | 4.1103 | -2.28 % |
| Liu [50] | 1.6308 ± 0.163 | -9.97 % | -------- | -------- |
| Rao et al. [51] | -------- | -------- | 4.4167 ± 0.402 | -9.06 % |

## 4. RESULTS OF GEOMETRICAL INVESTIGATION

The purpose is to obtain the maximization of the time, and spatial averaged ($\bar{q}'$) in the array and minimize ($\overline{C_D}$), applying the variation of the three degrees of freedom in the arrangement of bluff bodies, as explained previously. Considering the new degree of freedom introduced here is the ratio $H_1/L_1$, it is first evaluated the flow behavior as a function of $S_L/D$ and $S_T/D$ for fixed values of $H_1/L_1$. A thorough analysis is made for flows with $H_1/L_1$ = 0.1 and 5.0 since they are at the studied range's extreme magnitudes. The optimization study is also presented comprising all the steps of $H_1/L_1$ and its effect on $\overline{C_D}_{,2m}$, $\bar{q}'_{2m}$, and the corresponding optimal ratios of $(S_T/D)_{2o}$ and $(S_L/D)_o$.

### 4.1. Fluid dynamic and thermal analysis for $H_1/L_1$ = 0.1

Here, the geometric evaluation is presented for all studied cases where $H_1/L_1$ = 0.1. Due to the constructive characteristic of the domain geometry and its mesh, this case study does not comprehend the ratios $S_L/D$ = 2.0 with $S_T/D$ = 2.0, and $S_L/D$ = 2.5 with $S_T/D$ = 2.0. In these cases, there is an overlap of highly refined meshes in the bluff bodies region, caused by the proximity of the obstacles that prevented their correct generation. Therefore, the cases mentioned above were not solved. However, other results strongly infer that evaluating these two cases with a modified mesh would not bring impactful changes to the discussion that justified the effort, as can be seen in Fig. 5.

Figure 5 (a) illustrates the influence of $S_T/D$ on $\overline{C_D}$ considering several $S_L/D$. In general, the transverse pitch enlarges the drag coefficient in a linear form, especially between $S_T/D$ = 2.5 and 4.0. The exception is the case $S_L/D$ = 2.0, which presents a decrease in $\overline{C_D}$, also linear, in the same transverse spacing range. It can be deduced that, when the ratio of the longitudinal pitch is very small and the frontal body is quite elongated in the streamwise direction, the augmentation of the transverse pitch is

beneficial to reduction of $\overline{C_D}$. This behavior can be related to the need to generate more space to increase the bodies' momentum and minimize their pressure drop (see Figs. 6 and 7). In all other cases ($S_L/D \geq 2.5$), the frontal body's fluid dynamic has space enough to develop, generating a low pressure behind it, which benefits the decrease of flow resistance around the downstream bodies. For these cases, the increase in $S_T/D$ increases the $\overline{C_D}$ value since now a greater transverse spacing increases the free stream's incidence over the bodies. It can also be seen that the increase in longitudinal spacing also allows a reduction of $\overline{C_D}$ within the studied $S_T/D$ range. This behavior can be associated with the greater region of negative pressure behind the upstream body for the cases with higher magnitudes of $S_L/D$. The best case of $H_1/L_1$ = 0.1 is achieved when $(S_L/D)_{o,F}$ = 4.0, $(S_T/D)_{2o,F}$ = 2.0 with $\overline{C_D}_{,2m}$ 24.80% lower than that obtained with the worst case ($S_L/D$ = 2.0, $S_T/D$ = 2.5).

For thermal analysis, Fig. 5 (b) presents the effect of $S_T/D$ on the time and space-averaged ($\bar{q}'$). The increase in $\bar{q}'$ appears abruptly when $S_T/D$ changes for $S_T/D \leq 2.5$. However, it tends to practically suffer no changes between $S_T/D$ = 3.0 and 4.0. Part of this can be explained by the thermal boundary layer pattern generated by the elongated upstream body, which causes a strong interaction with the downstream bodies when $S_T/D \leq 2.5$. Moreover, in this case, differences of momentum caused by $S_T/D$ variation in the range ($3.0 \leq S_T/D \leq 4.0$) are not significant. In this analysis, the best case is obtained with $(S_L/D)_{o,T}$ = 2.0 and $(S_T/D)_{2o,T}$ = 4.0 leading to $\bar{q}'$ 13.54% superior than that achieved with the worst case, $S_L/D$ = 4.0 and $S_T/D$ = 2.0.

Figures 6 and 7 present the velocity and pressure fields for selected cases ($H_1/L_1$ = 0.1 and $S_L/D$ = 4.0) to illustrate the general flow pattern when the transverse spacing of the posterior obstacles varies. Note that, in Fig. 6 (a), there is a large range of low-speed flow downstream of the arrangement. Moreover, few of the free stream has direct incidence over the downstream bodies. When the transverse spacing increases as in Figs. 6 (b) – (d) and Figs. 7 (b) – (d), the flow is accelerated in the arrangement's interstices, reducing the low-velocity zone and consequently the distance where high and low pressures happened in the arrangement. The velocity and pressure fields corroborated the previous statement that the lowest magnitude of $S_T/D$ = 2.0 allowed the generation of a large region of the pressure gradient in comparison with other magnitudes of $S_T/D$, i.e., the best shape is the one which best distributes the velocity and pressure fields in the arrangement. Figure 7 also clearly illustrates that the high-pressure region in front of the

bluff bodies is strongly reduced for the lowest magnitude of $S_T/D$, Fig. 7 (a), in comparison with the others, Figs. 7 (b) – (d).

To conclude the analysis for the cases with $H_1/L_1$ = 0.1, Fig. 8 depicts the thermal fields for the same cases presented for velocity and pressure fields in Figs. 6 and 7. It can be noticed a clear difference among the thermal fields of Fig. 8 (a) and Figs. 8 (b) – (d). When $S_T/D$ = 2.0, Fig. 8 (a), a concentrated region of hot temperatures near the arrangement of bodies can be observed. Once the fluid flow is restricted among the bodies, the energy transfer from the central region of the domain towards the two peripheral fresh streams is composed of few branches of vortex structures concentrated in the central region behind the cylinders. As the ratio $S_T/D$ increases, the momentum between posterior bodies is augmented.

Consequently, the central hot stream has more intensity to transfer energy from central to peripheral fresh streams, generating complex tree-shaped branches (vortex structures) behind the arrangement. These interactions are generated by interaction among von Karman vortex streets behind the bodies. In general, results indicated that the thermal fields' design changed to augment the internal currents of heat from the highest potential (central portion of the channel) towards the lowest one (peripheral region), i.e., easily the internal currents in the flow system. Moreover, the tree-shaped structures of thermal fields depend on the flow intensity among the cylinders. The differences noticed in the thermal fields affected the $\bar{q}'$ in the arrangement for different $S_T/D$ magnitudes.

### 4.2. Fluid dynamic and thermal analysis for $H_1/L_1$ = 5.0

Figures 9(a) and 9(b) presented the influence of $S_T/D$ over $\overline{C_D}$ and $\bar{q}'$ for $H_1/L_1$ = 5.0, respectively. Generally, it is observed an increase of $\overline{C_D}$ and $\bar{q}'$ for different magnitudes of $S_L/D$. Concerning the thermal objective, a curious result is also observed, an inflection in the curve of $\bar{q}'$ that occurs for almost all $S_L/D$, as illustrated in Fig. 9 (b). As the transverse spacing increases from $S_T/D$ = 2.0 to 2.5, $\bar{q}'$ undergoes a small, but noticeable reduction in almost all cases. The exception is $S_L/D$ = 2.0, which presents a variation of the same order, but with a growth of $\bar{q}'$. From $S_T/D$ = 2.5 and up, the averaged linear heat flux curve corresponds to the drag coefficient curve (Fig. 9 (a)) for each case, showing successive growth while $S_T/D$ increases. It is worth mentioning that higher e magnitudes of $S_T/D$ are not investigated due to restrictions imposed by the occupation

area. It is also interesting to note in Fig. 9 (b) that especially for $\bar{q}'$ the flow is practically insensitive to longitudinal spacing, since the different $S_L/D$ curves practically overlap between $S_T/D$ = 3.0 and 4.0, having a total mean relative deviation slightly less than 5% in the whole evaluated range. Finally, for the drag coefficient with $H_1/L_1$ = 5.0, the best case, $(S_L/D)_{o,F}$ = 4.0 and $(S_T/D)_{2o,F}$ = 2.0, has a performance 61.09 % superior than the case with the worst performance ($S_L/D$ = 2.0 and $S_T/D$ = 4.0). When $\bar{q}'$ is the performance indicator, the best case is obtained for $(S_L/D)_{o,T}$ = 3.5, and $(S_T/D)_{2o,T}$ = 4.0. The best configuration performed 88.07% better than the worst one, showing that the optimal configurations for the arrangement are strongly affected by the upstream body's shape.

Figs. 10 and 11 illustrate the fields of velocity and pressure when $H_1/L_1$ = 5.0. The frontal obstacle presents itself too much of a barrier, almost as a protective shield for the posterior bluff bodies, which makes the flow pass by them with minimal velocity and thus minimizing the heat transfer. With $S_T/D \leq 2.5$, the downstream obstacles are practically behind the upstream one. This panorama changes when the transverse spacing increases as the flow starts to hit the posterior bluff bodies' face. When doing this, for $S_T/D \geq 3.0$, the flow can manage to pass in between the posterior obstacles increasing the momentum among the bodies. The pressure fields also demonstrate a strong increase of pressure in front of the obstacles as the ratio $S_T/D$ increases, including in the downstream bodies.

Figure 12 illustrates some selected temperature fields, where it is possible to see the reason why even when $S_T/D$ = 4.0, $\bar{q}'$ does not show signs of reaching a maximum value for the arrangement since even in this transverse spacing, the thermal boundary layer of each bluff body interferes widely in the layers of the others. In other words, at any moment, the obstacles do not appear to be isolated in the flow, which occurred in Teixeira et al. [44] for large transverse spacing ratios and small longitudinal spacing ratios, when all obstacles are square-shaped. Results of thermal fields also demonstrated that, for all $S_T/D$ magnitudes, the arrangement generated Kelvin Helmholtz instabilities followed by von Karman vortex streets.

Concluding the individual thermal and fluid dynamics analyzes, the other cases of $H_1/L_1$ presented the expected and most predictable behaviors, where the increase in transverse and longitudinal spacing leads to the proportional growth of $\overline{C_D}$ and $\bar{q}'$. It is worth noting that for the intermediate values of $H_1/L_1$, the curves' behavior followed the trends. For example, in $H_1/L_1$ = 0.5, the increase in the transversal spacing takes the curves of $\overline{C_D}$ and $\bar{q}'$ to what is assumed peak values with little variation between $S_T/D$ = 3.0 and 4.0 as with $H_1/L_1$ = 0.1. The same can be said when $H_1/L_1$ = 2.0 compared to $H_1/L_1$ = 5.0

because, in these cases, the increase in the transverse spacing keeps the curves of $\overline{C_D}$ and $\bar{q}'$ similar to that noticed for $H_1/L_1$ = 5.0. Then, for the sake of brevity, these effects are not reproduced here.

### 4.3. Complete optimization and multi-objective study

Here, the complete optimization of the triangular arrangement for different magnitudes of $H_1/L_1$ is carried out. As previously mentioned, the main purposes are the minimization of $\overline{C_D}$ (fluid dynamic objective) and maximization of $\bar{q}'$ (thermal objective). These two objectives are competing, since, in general, the maximization or minimization of one generates the same proportional reaction in the other. However, as seen in similar previous works [32 - 35], this behavior is not always linear, and it is possible to find the optimal geometric ratios that best meet both objectives concurrently, with the least compromise between them.

First, it is realized the study of each objective. Figures 13(a) and 13 (b) summarize and present the optimal configurations achieved in Figs. 5 (a) and 9 (a). Moreover, results for the best shapes reached for the ratios $H_1/L_1$ = 0.5, 1.0, and 2.0 are also presented. More precisely, Figs. 13 (a) and 13 (b) show the effect of $S_L/D$ over $\overline{C_D}_{,m}$, and optimal correspondent ratio $(S_T/D)_{o,F}$ for different ratios of $H_1/L_1$, respectively. Fig. 13 (a) shows that the $H_1/L_1$ = 0.1 and 5.0 ratios actually present the least predictable behaviors for $\overline{C_D}_{,m}$, and also less desirable, since they present values much higher than the other ratios in almost all of the studied range of $S_L/D$. The ratio $H_1/L_1$ = 2.0 has the lowest values for all $\overline{C_D}_{,m}$ for all longitudinal spacing studied. It is also easily observed that the lowest values of $\overline{C_D}_{,m}$ for each curve is found in $S_L/D$ = 4.0. Figure 13 (b) shows that the transverse pitch, once optimized for the fluid dynamic purpose for almost all $H_1/L_1$ ratios regardless $S_L/D$ value, is obtained for $(S_T/D)_{o,F}$ = 2.0. The only exception is the case with $H_1/L_1$ = 0.1, with higher distances between downstream bodies conducted to the lowest values of $\overline{C_D}_{,m}$ when $S_L/D$ = 2.0.

A similar analysis for the heat transfer aim is shown in Figs. 14 (a) and (b) and illustrates the effect of the $S_L/D$ ratio over $\bar{q}'_m$ and the corresponding optimal transverse pitch ratio for the thermal purpose, $(S_T/D)_{o,T}$. The ratios of $H_1/L_1$ = 0.1 and 5.0 present again the highest magnitudes looking at Fig. 14 (a). However, here this is a positive behavior since the maximization of $\bar{q}'_m$ is sought. In fact, $H_1/L_1$ = 0.1 is at least 16%

higher than the second best-case ($H_1/L_1$ = 5.0). Moreover, the best shapes for all cases are obtained when $(S_L/D)_{o,T}$ = 2.0. Similar to the fluid dynamic study, Fig. 14 (b) illustrates that $(S_T/D)_{o,T}$ is constant regardless of $S_L/D$ for almost all $H_1/L_1$ ratios. For the thermal study, the highest magnitudes are $\bar{q}'_{2m}$ and the corresponding optimal ratios for the thermal purpose are $(S_T/D)_{2o,T}$ and $(S_L/D)_{o,T}$. In general, for the present conditions, results indicated that most close bodies in the downstream direction are beneficial for the thermal purpose, while more apart bodies in the same direction are more suitable for the fluid dynamic purpose. For the transverse pitch, the best fluid dynamic configurations are achieved for the transverse pitch's lowest magnitudes. Conversely, the optimal shape for thermal purpose is reached when the bodies are most apart, and the upstream body is elongated ($H_1/L_1$ = 0.1).

Finally, the best shapes reached in Figs. 13 and 14 are summarized in Fig. 15. More precisely, Figs. 15(a) and 15(b) show the influence of $H_1/L_1$ over $\overline{C_D}_{,2m}$ and $\bar{q}'_{2m}$, and the corresponding optimal shapes, respectively. Results of Fig. 15(a) show that the best configuration for the fluid dynamic performance is reached at an intermediate ratio of $H_1/L_1$. Therefore, the best fluid dynamic shape is reached for $(H_1/L_1)_{o,F}$ = 2.0; $(S_L/D)_{2o,F}$ = 4.0 and $(S_T/D)_{3o,F}$ = 2.0, being its $\overline{C_D}_{,3m}$ 19.94% lower than the worst $\overline{C_D}_{,2m}$. The optimized transverse and longitudinal ratios remain constant throughout the range of $H_1/L_1$ in the fluid dynamics performance indicator. For the thermal case, Fig. 15 (b), the difference between the worst and the best $\bar{q}'_{,2m}$ is 33.29%, indicating a higher sensibility of $H_1/L_1$ for the thermal problem. The optimal spacing ratios between bluff bodies are practically reversed, while the optimum shape ratio of the upstream obstacle is seen when the shape is the most slender studied, that is, $\bar{q}'_{,3m}$ is found in $(H_1/L_1)_{o,T}$ = 0.1; $(S_L/D)_{2o,T}$ = 2.0 and $(S_T/D)_{3o,T}$ = 4.0. Unlike what is observed for the fluid dynamics, here, the ratio of the longitudinal spacing once optimized is not constant for all $H_1/L_1$, ranging from $(S_L/D)_{o,T}$ = 2.0 to 3.5 between $H_1/L_1$ = 2.0 and 5.0.

Figures 16 and 17 illustrate the fields of velocity, pressure, and temperature for the optimal fluid dynamic and thermal cases, respectively. It can be seen in Figs. 16 (a) - (c), that the flow has a very regular behavior, with the first body being high to reduce the pressure magnitude in front of downstream bodies, but not enough to hide them. Then, this shape of the frontal obstacle combined with transverse and longitudinal spacing helps to reduce drag, as it does not represent as much of a barrier. On the other hand, Figs. 17 (a) - 17 (c) show the velocity, pressure, and thermal fields for the best shape for thermal

performance. As previously mentioned, the elongated frontal body is good to better distribute the momentum among the bodies allowing the increase of energy transfer from the central heated region of domain towards the fresh peripheral regions of the domain by the interaction of von Karman vortex streets generated behind both downstream bodies.

The final evaluation to be carried out is the multi-objective study, in which it is sought to determine the design that best favors the two objectives (thermal and fluid dynamics) of the study, concomitantly. As the parameters evaluated have different orders of magnitude, normalization is performed to represent the results visually better and more significantly. Besides, as the objectives are opposite ($\overline{C_D}$ seeks minimization and $\bar{q}'$ maximization) the comparison of a normalized value is made according to the inverse of the other normalized value. That said, the drag coefficient is normalized in a $\overline{C_D}/\overline{C_D}_{,2m}$ fashion, while the heat transfer rate is made $(\bar{q}'/\bar{q}'_{2m})^{-1}$. Thus it is possible to evaluate the recommended design for both performance indicators. Figure 18 shows exactly this evaluation. Another interesting issue in evaluating this way is that the origin comes to represent the hypothetical ideal case where the drag coefficient would be zero and the heat transfer infinite. Therefore, the closer to the origin, the closer to the ideal point the case is. Therefore, a parameter called the ideal point distance ($\Delta i$) is used in Fig. 18, which is the distance from the origin to the value of the case under analysis. Note that $H_1/L_1$ = 0.1 has the smallest $\Delta i$, which puts the optimal thermal case as the optimal multi-objective case. This result is one indication that, for the present problem, the design has more sensibility over the thermal than fluid dynamic performance.

## 5. CONCLUSIONS

In this study, the Constructal Design method was applied to investigate the geometric configuration of a triangular array of bluff bodies under forced convective flows in the laminar regime. The effect the frontal body's design over both performance indicators studied here ($\overline{C_D}$ and $\bar{q}'$) and its influence over the transverse and longitudinal pitch of the array was considered.

Results indicated that the performance indicators are strongly affected by the array configurations and height/length ratio of the upstream body for the present simulated conditions. Moreover, regardless of the performance indicator, the system was strongly

improved with design investigation. For minimization of $\overline{C_D}$, the optimal shape obtained with $(H_1/L_1)_{o,F}$ = 2.0; $(S_L/D)_{2o,F}$ = 4.0 and $(S_T/D)_{3o,F}$ = 2.0 led to $\overline{C_D}_{,3m}$ 68.9% inferior than that reached for the worst case. For the thermal purpose, the optimal shape obtained with $(H_1/L_1)_{o,T}$ = 0.1, $(S_L/D)_{2o,T}$ = 2.0 and $(S_T/D)_{3o,T}$ = 4.0 conducted to $\bar{q}'_{,3m}$ 100.3% superior than the worst case. These results proved the applicability of Constructal Design as a tool for the design of external flow arrangements.

Results also showed the three degrees of freedom ($S_T/D$, $S_L/D$, and $H_1/L_1$) presented important influence over the performance indicators. Moreover, changes in the frontal body ($H_1/L_1$) were significant for the influence of $S_T/D$ and $S_L/D$ in the performance indicators ($\overline{C_D}$ and $\bar{q}'$). The optimal thermal performance was achieved for tree-shaped thermal streams composed of a complex interaction between von Karman vortex streets behind downstream bodies, i.e., the design of thermal streams configured itself to maximize the currents from the central heated portion of domain towards the peripheral fresh streams. To summarize, the multi-objective evaluation pointed to a dominance of the thermal problem for the conditions studied here, since the optimum thermal case is also the optimum multi-objective case.

For future studies, the design of the arrangement subjected to other working fluids and conditions (e.g., other Reynolds numbers, mixed convection, and turbulent flows) are recommended.

## 6. ACKNOWLEDGEMENTS

F. B. Teixeira thanks CNPq for the doctorate scholarship. C. Biserni is sponsored by the Italian Ministry for Education, University and Research. E.D. dos Santos, L.A. Isoldi, and L.A.O. Rocha thank CNPq (Brasília, DF, Brazil) for the research Grant (Processes: 306024/2017-9, 306012/2017-0 and 307791/2019-0). All authors thank FAPERGS for financial support in PqG Program – Notice Nº 05/2019 (Process: 19/2551-0001847-9).

## 7. REFERENCES

[1] M. Zdravkovich, Flow Around Circular Cylinders, Oxford University Press Inc., New York, 1997.

[2] D. Sumner, Two circular cylinders in cross-flow: a review, J. Fluids Struct. 26 (2010) 849 – 899, https://doi.org/10.1016/j.jfluidstructs.2010.07.001.

[3] J.F. Derakhshandeh, Md M. Alam, A review of bluff body wakes, Ocean Eng. 182 (2019) 475 – 488, https://doi.org/10.1016/j.oceaneng.2019.04.093

[4] J.P. Dulhani, S. Sarkar, A. Dalal, Effect of angle of incidence on mixed convective wake dynamics and heat transfer past a square cylinder in cross flow at *Re* = 100, Int. J. Heat Mass Tran. 78 (2014) 319 – 332, https://doi.org/10.1016/j.ijheatmasstransfer.2014.03.021.

[5] A. Shadlaghani, M.R. Tavakoli, M. Farzaneh, M.R. Salimpour, Optimization of triangular fins with/without longitudinal perforate for thermal performance enhancement, J. Mech. Sci. Technol. 30 (4) (2016) 1903 – 1910, https://doi.org/10.1007/s12206-016-0349-5.

[6] C.C. Liao, C.A. Lin, Influences of a confined elliptic cylinder at different aspect ratios and inclinations on the laminar natural and mixed convection flows, Int. J. Heat Mass Tran. 55 (2012) 6638 – 6650, https://doi.org/10.1016/j.ijheatmasstransfer.2012.06.073.

[7] W.M. El-Maghlany, M.A. Alnakeeb, M.A. Teamah, M.M. Sorour, Experimental and numerical study of laminar mixed convection from a horizontal isothermal elliptic cylinder, Int. J. Therm. Sci. 130 (2018) 116 – 127, https://doi.org/10.1016/j.ijthermalsci.2018.04.018.

[8] C.G. Patel, S. Sarkar, S.K. Saha, Mixed convective vertically upward flow past side-by-side square cylinders at incidence, Int. J. Heat Mass Tran. 127 (2018) 927 – 947, https://doi.org/10.1016/j.ijheatmasstransfer.2018.06.129.

[9] A. Dhiman, R. Ghosh, Computer simulation of momentum and heat transfer across an expanded trapezoidal bluff body, Int. J. Heat Mass Tran. 59 (2013) 338 – 352, https://doi.org/10.1016/j.ijheatmasstransfer.2012.12.031.

[10] H.J. Schmidt, R. Woszidlo, C.N. Nayeri, C.O. Paschereit, Drag reduction on a rectangular bluff body with base flaps and fluidic oscillators, Exp. Fluids (2015) 56 – 151, https://doi.org/10.1007/s00348-015-2018-3.

[11] S. Bouzari, J. Ghazanfarian, Unsteady forced convection over cylinder with radial fins in cross flow, Appl. Therm. Eng. 112 (2017) 214 – 225, https://doi.org/10.1016/j.applthermaleng.2016.10.052.

[12] S. Li, T. Zhou, Z. Sun, Z. Dong, External forced convection from circular cylinders with surface protrusions, Int. J. Heat Mass Tran. 99 (2016) 20 – 30,

https://doi.org/10.1016/j.ijheatmasstransfer.2016.03.092.

[13] A. Kumar, A. Dhiman, L. Baranyi, Fluid flow and heat transfer around a confined semi-circular cylinder: onset of vortex shedding and effects of Reynolds and Prandtl numbers, Int. J. Heat Mass Tran. 102 (2016) 417 – 425, https://doi.org/10.1016/j.ijheatmasstransfer.2016.06.026.

[14] P.M. Patil, A. Shashikant, S. Roy, P.S. Hiremath, Mixed convection flow past a yawed cylinder, Int. Commun. Heat Mass Tran. 114 (2020) 104582, https://doi.org/10.1016/j.icheatmasstransfer.2020.104582.

[15] Z. Wang, D.S.-K. Ting, R. Carriveau, W. Xiong, Z. Wang, Numerical and experimental investigation of flow around a balloon-shaped bluff body, Sustain. Energy Techn. 35 (2019) 80 – 88, https://doi.org/10.1016/j.seta.2019.06.005.

[16] A.P. Pawar, S. Sarkar, S.K. Saha, Forced convective flow and heat transfer past an unconfined blunt headed cylinder at different angles of incidence, Appl. Math. Model. 82 (2020) 888 – 915, https://doi.org/10.1016/j.apm.2020.01.067.

[17] Y. Gao, X. Qu, M. Zhao, L. Wang, Three-dimensional numerical simulation of flow past three circular cylinders in an equilateral-triangular arrangement, Ocean Eng. 189 (2019) 106375, https://doi.org/10.1016/j.oceaneng.2019.106375.

[18] R. Pravesh, A. Dhiman, R.P. Bharti, Aiding buoyancy mixed convection flow and thermal features across a periodic array of heated cylinders, Int. J. Heat Mass Tran. 130 (2019) 1141 – 1162, https://doi.org/10.1016/j.ijheatmasstransfer.2018.11.035.

[19] W. Zhang, X. Chen, H. Yang, H. Liang, Y. Wei, Forced convection for flow across two tandem cylinders with rounded corners in a channel, Int. J. Heat Mass Tran. 130 (2019) 1053 – 1069, https://doi.org/10.1016/j.ijheatmasstransfer.2018.10.125.

[20] C.G. Patel, S. Sarkar, S. Kumarsaha, Mixed convective vertically upward flow past side-by-side square cylinders at incidence, Int. J. Heat Mass Tran. 127 (2018) 927-947, https://doi.org/10.1016/j.ijheatmasstransfer.2018.06.129.

[21] D. Sumner, H.K. Reitenbach, Wake interference effects for two finite cylinders: a brief review and some new measurements, J. Fluids Struct. 89 (2019) 25 – 38, https://doi.org/10.1016/j.jfluidstructs.2019.02.004.

[22] A. Bejan, Advanced Engineering Thermodynamics, 2nd edition, John Wiley, New York, 1996.

[23] A. Bejan, Shape and Structure, from Engineering to Nature, Cambridge University Press, Cambridge, 2000.

[24] A. Bejan, S. Lorente, Design with Constructal Theory, Wiley, Hoboken, 2008.

[25] A. Bejan, P. Zane, Design in nature: how the constructal law governs evolution in biology, physics, technology, and social organization, 1st edition, Doubleday, New York, 2012.

[26] A. Bejan, The physics of life: the evolution of everything, St. Martins Press, New York, 2016.

[27] A. Bejan, Evolution in thermodynamics, Appl. Phys. Rev. 4 (1) (2017) 011305. https://doi.org/10.1063/1.4978611.

[28] T. Bello-Ochende, A. Bejan, Constructal multi-scale cylinders with natural convection, Int. J. Heat Mass Tran. 48 (2005) 4300 – 4306, https://doi.org/10.1016/j.ijheatmasstransfer.2005.05.023.

[29] Y. Kim, S. Lorente, A. Bejan, Constructal multi-tube configuration for natural and forced convection in cross-flow, Int. J. Heat Mass Tran. 53 (23–24) (2010) 5121 – 5128, https://doi.org/10.1016/j.ijheatmasstransfer.2010.07.053.

[30] T. Bello-Ochende, J.P. Meyer, O.I. Ogunronbi, Constructal multiscale cylinders rotating in cross-flow, Int. J. Heat Mass Tran. 54 (2011) 2568–2577, https://doi.org/10.1016/j.ijheatmasstransfer.2011.02.004.

[31] L.G. Page, T. Bello-Ochende, J.P. Meyer, Constructal multi scale cylinders with rotation cooled by natural convection, Int. J. Heat Mass Tran. 57 (2013) 345 – 355, https://doi.org/10.1016/j.ijheatmasstransfer.2012.10.048.

[32] G.M. Barros, G. Lorenzini, L.A. Isoldi, L.A.O. Rocha, E.D. dos Santos, Influence of mixed convection laminar flows on the geometrical evaluation of a triangular arrangement of circular cylinders, Int. J. Heat Mass Tran. 114 (2017) 1188 – 1200, https://doi.org/10.1016/j.ijheatmasstransfer.2017.07.010.

[33] F.B. Teixeira, G. Lorenzini, M.R. Errera, L.A.O. Rocha, L.A. Isoldi, E.D. dos Santos, Constructal Design of triangular arrangements of square bluff bodies under forced convective turbulent flows, Int. J. Heat Mass Tran. 126 (2018) 521 – 535, https://doi.org/10.1016/j.ijheatmasstransfer.2018.04.134.

[34] B.C. Feijó, G. Lorenzini, L.A. Isoldi, L.A.O. Rocha, J.N.V. Goulart, E.D. dos Santos, Constructal design of forced convective flows in channels with two alternated rectangular heated bodies, Int. J. Heat Mass Tran. 125 (2018) 710 – 721, https://doi.org/10.1016/j.ijheatmasstransfer.2018.04.086.

[35] F.B. Teixeira, M.V. Altnetter, G. Lorenzini, B.D.A. Rodriguez, L.A.O. Rocha, L.A. Isoldi, E.D. dos Santos, Geometrical Evaluation of a Channel with Alternated Mounted Blocks under Mixed Convection Laminar Flows Using Constructal

Design, J. Eng. Thermophys. 29 (1) (2020) 92 – 113, https://doi.org/10.1134/S1810232820010087.

[36] D. Jing, S. Yi, Electroosmotic flow in tree-like branching microchannel network, Fractals 27 (6) (2019) 1950095. https://doi.org/10.1142/S0218348X19500956

[37] D. Jing, J. Song, Y. Sui, Hydraulic and thermal performances of laminar flow in fractal treelike branching microchannel network with wall velocity slip, Fractals 28 (2) (2020) 2050022. https://doi.org/10.1142/S0218348X2050022X.

[38] ANSYS. 18.1. – FLUENT User's Guide, ANSYS Inc. 2017.

[39] H.K. Versteeg, W. Malalasekera, An Introduction to Computational Fluid Dynamics – The Finite Volume Method, 2nd edition, Longman, 2007.

[40] S,V, Patankar, Numerical Heat Transfer and Fluid Flow, McGraw-Hill, New York, 1980.

[41] E.S.D. Estrada, E.X. Barreto, L.A. Isoldi, E.D. dos Santos, S. Lorente, L.A.O. Rocha, Constructal design of tree shaped cavities inserted into a cylindrical body with heat generation. Int. J. Therm. Sci. 152 (2020) 106342 – 106342-10, https://doi.org/10.1016/j.ijthermalsci.2020.106342.

[42] A. Bejan, Convection Heat Transfer, 4th edition, John Wiley, Durham, 2013. https://doi.org/10.1002/9781118671627.

[43] A.K. Sahu, R.P. Chhabra, V. Eswaran, Effects of Reynolds and Prandtl numbers on heat transfer from a square cylinder in the unsteady flow regime, Int. J. Heat Mass Tran. 52 (2009) 839 –850, https://doi.org/10.1016/j.ijheatmasstransfer.2008.07.032.

[44] F.B. Teixeira, M.S. Pereira, B.C. Feijó, L.A.O. Rocha, J.N.V. Goulart, T. Melo, L.A. Isoldi, E.D. dos Santos, Geometrical optimization of forced convective flows over an triangular arrangement of square bluff bodies (*in portuguese*), Rev. Int. Pesq. Eng. - RIPE 2 (2016) 101 – 113, https://doi.org/10.26512/ripe.v2i32.14428.

[45] A. Sharma, V. Eswaran, Heat and fluid flow across a square cylinder in the two-dimensional laminar flow regime, Numer. Heat Tran. A 45 (3) (2004) 247 – 269. https://doi.org/10.1080/10407780490278562.

[46] A. Sohankar, C. Norberg, L. Davidson, Low-Reynolds-number flow around a square cylinder at incidence: study of blockage, onset of vortex shedding and outlet boundary condition, Int. J. Num. Meth. Fluid. 26 (1998) 39 – 56. https://doi.org/10.1002/(SICI)1097-0363(19980115)26:1<39::AID-FLD623>3.0.CO;2-P.

[47] C. Norberg, Flow around rectangular cylinders: pressure forces and wake

frequencies, J. Wind Eng. Ind. Aerodyn. 49 (1993) 187 – 196. https://doi.org/10.1016/0167-6105(93)90014-F.

[48] S. Tanweer, A. Dewan, S. Sanghi, Study on effects of Prandtl number on cross buoyancy flow past a square cylinder using OpenFOAM, J. Appl. Fluid Mech. 12 (1) (2019) 257 – 269. https://doi.org/10.18869/acadpub.jafm.75.253.29020.

[49] S. Turki, H. Abbassi, S. Nasrallah, Two-dimensional laminar fluid flow and heat transfer in a channel with a built-in heated square cylinder, Int. J. Therm. Sci 42 (2003) 1105 – 1113. https://doi.org/10.1016/S1290-0729(03)00091-7.

[50] R. Liu, Flow around bluff bodies with corner modifications on cross-sections, Master Dissertation Thesis, University of New Hampshire, 2019.

[51] P.K. Rao, C. Sasmal, A.K. Sahu, R.P. Chhabra, V. Eswaran, Effect of power-law fluid behavior on momentum and heat transfer characteristics of an inclined square cylinder in steady flow regime, Int. J. Heat Mass Tran. 54 (2011) 2854 – 2867. https://doi.org/10.1016/j.ijheatmasstransfer.2011.03.013.

## FIGURE CAPTION LIST

Figure 18 Normalized values for $\overline{C_{D,2m}}$ versus the normalized inverse $\overline{q'}_{2m}$ for various $H_1/L_1$.

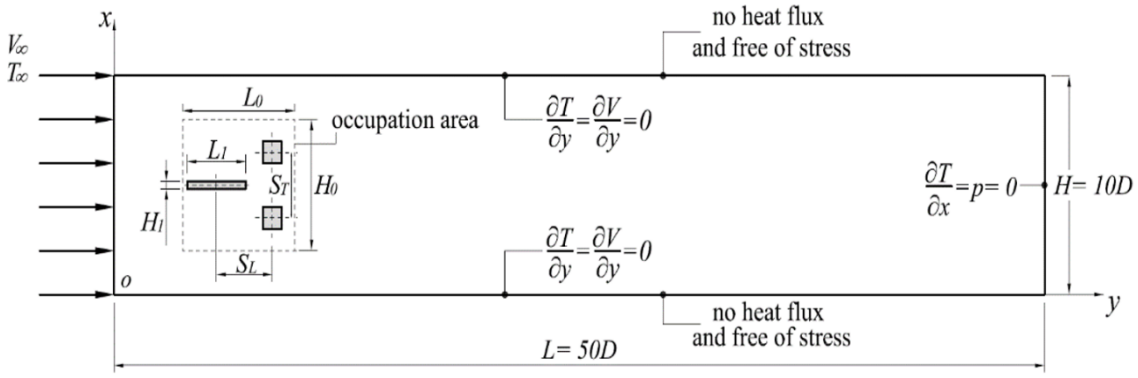


Figure 1 – Computational domain of the present work.

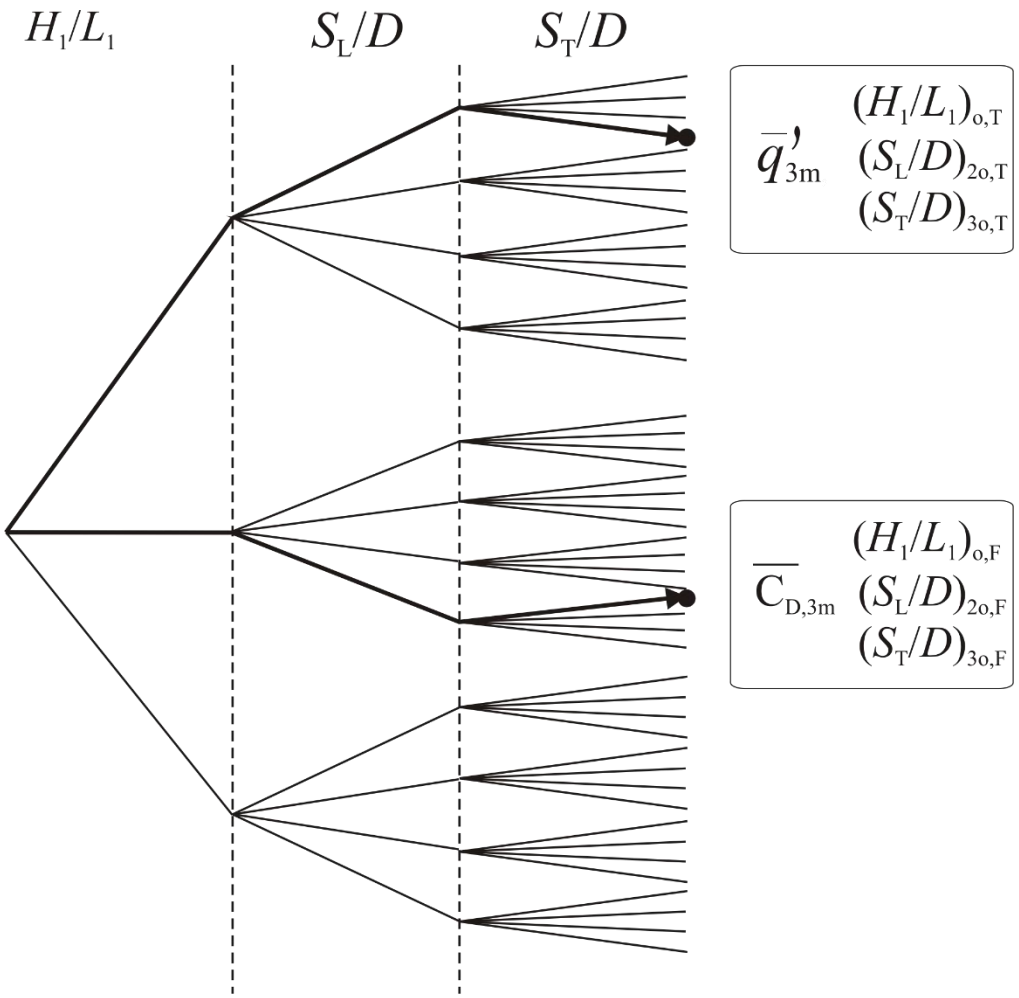


Figure 2 – Flowchart of Constructal Design method employed for geometrical investigation of the problem.

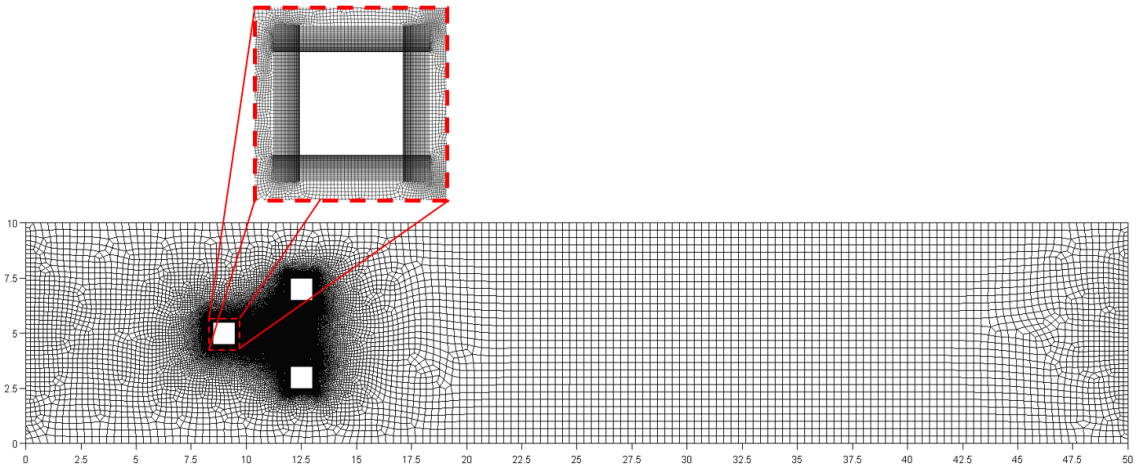


Figure 3 – Spatial discretization of domain and refinement in the bluff body.

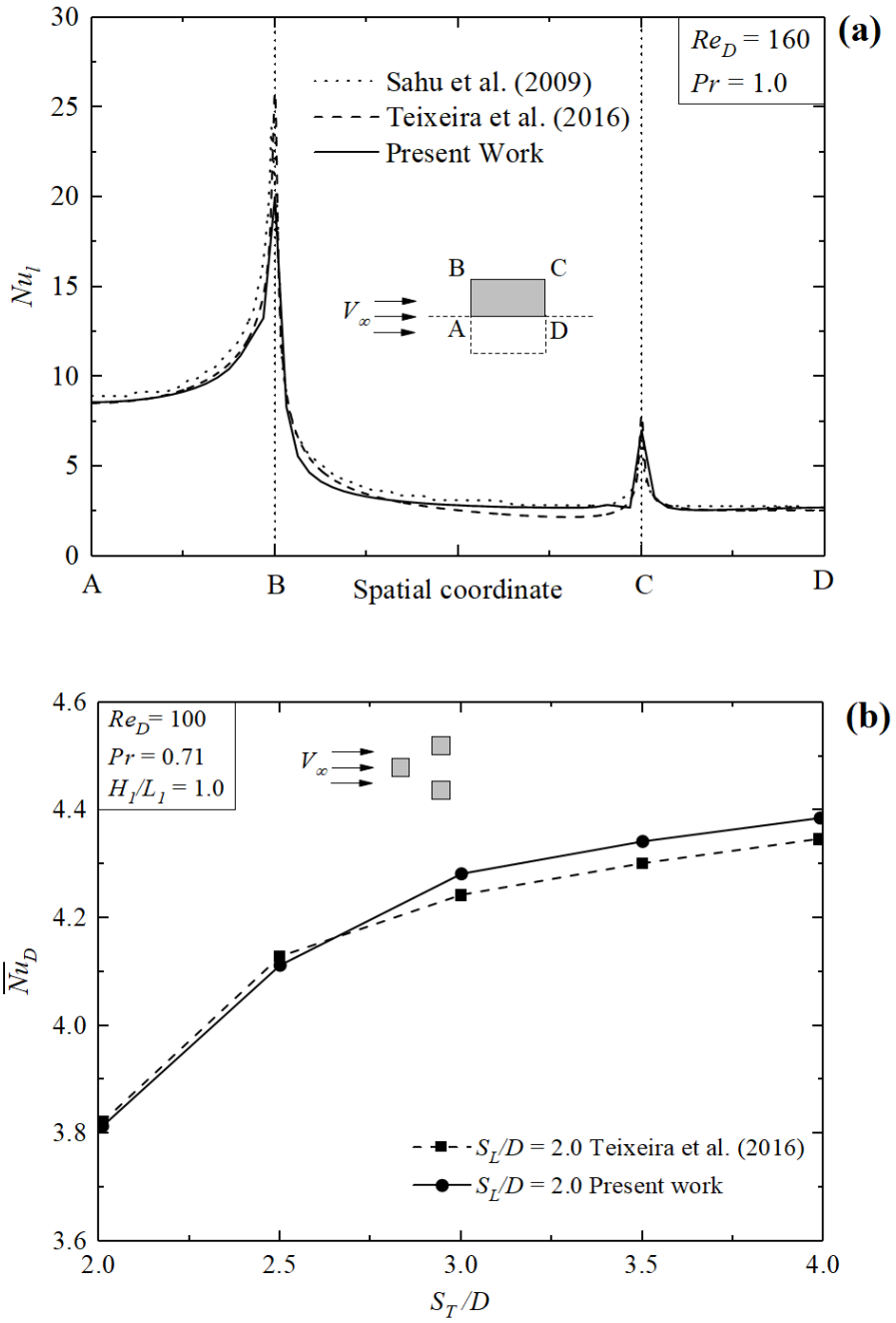


Figure 4 – Verification study for (a) local Nusselt number on a single body, (b) time averaged Nusselt number over the arrangement.

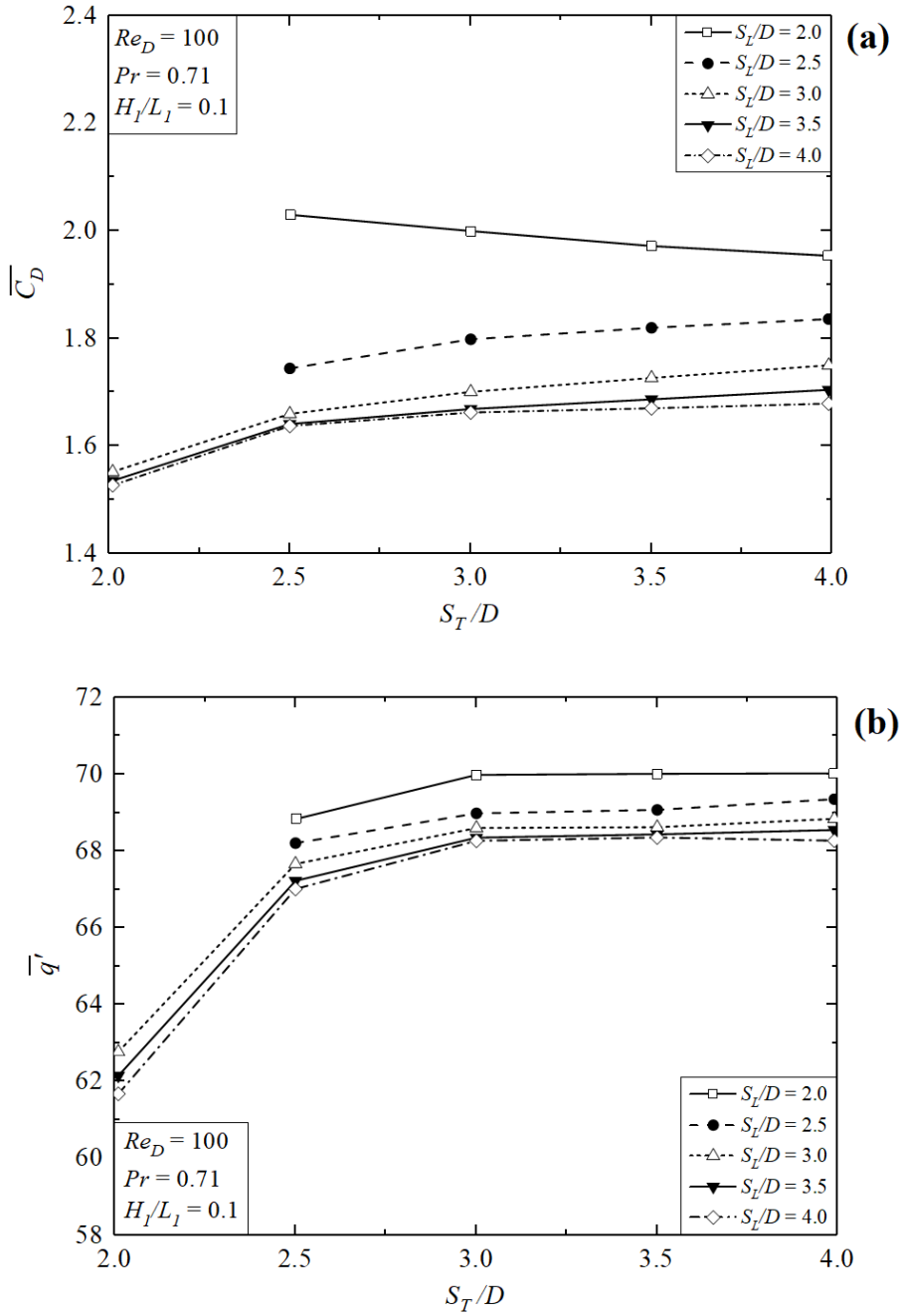


Figure 5 – Effect of $S_T/D$ over performance indicator for various values of $S_L/D$ and $H_1/L_1 = 0.1$: (a) drag coefficient and (b) heat transfer rate per unit length.

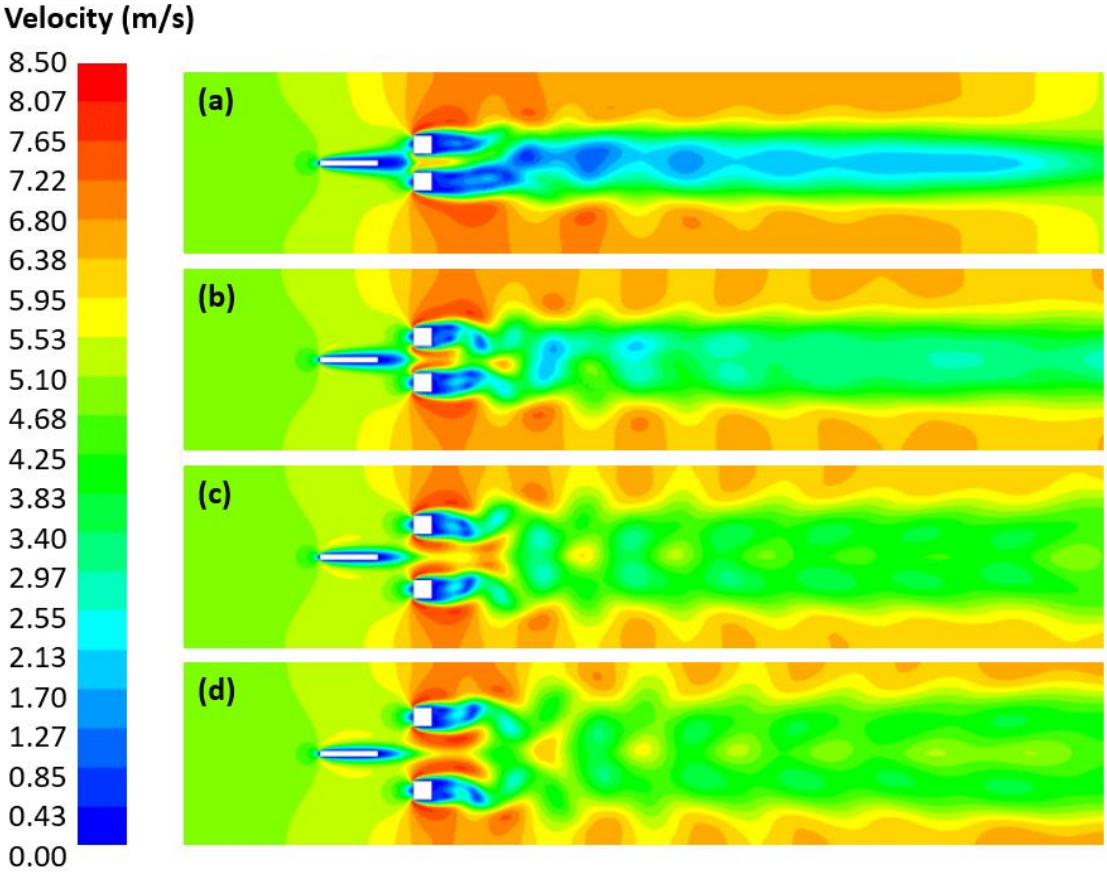


Figure 6 – Fields of velocity for $H_1/L_1$ = 0.1, $S_L/D$ = 4.0 and: (a) $S_T/D$ = 2.0, (b) $S_T/D$ = 2.5, (c) $S_T/D$ = 3.0 and (d) $S_T/D$ = 4.0.

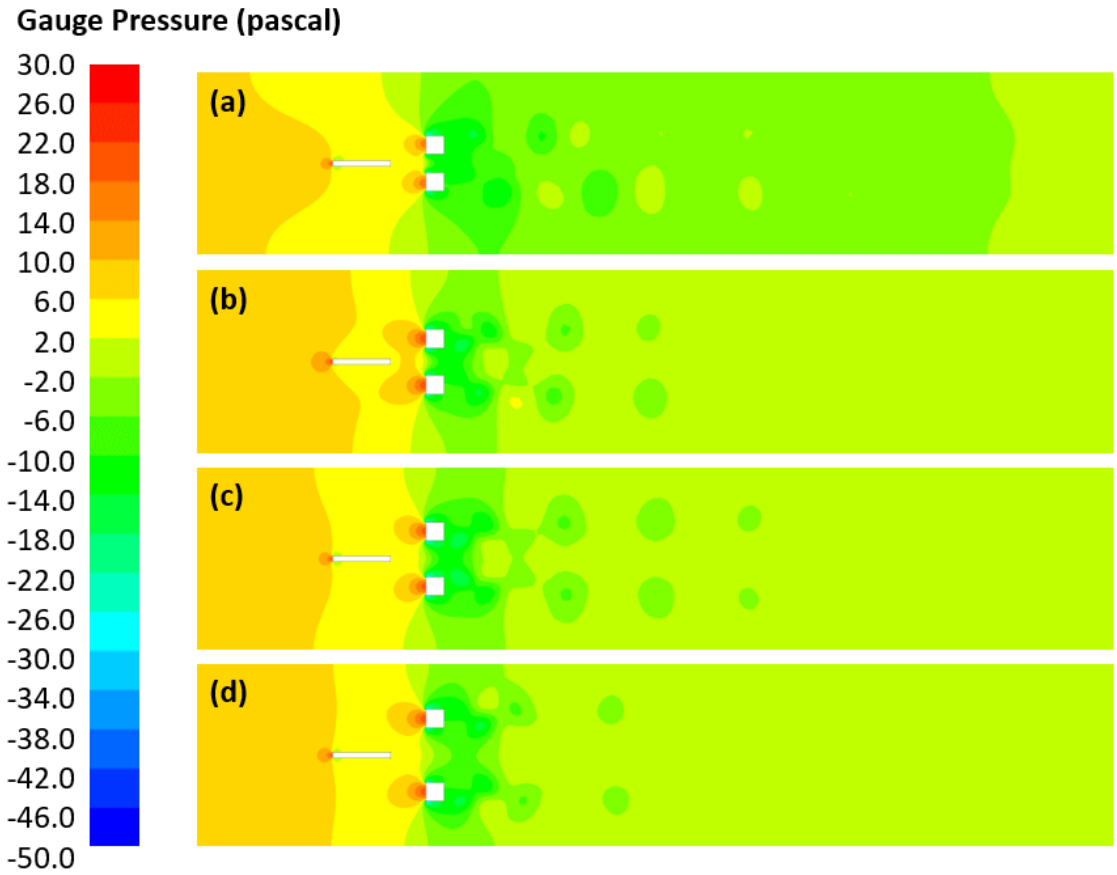


Figure 7 - Fields of pressure for $H_1/L_1$ = 0.1, $S_L/D$ = 4.0 and: (a) $S_T/D$ = 2.0, (b) $S_T/D$ = 2.5, (c) $S_T/D$ = 3.0 and (d) $S_T/D$ = 4.0.

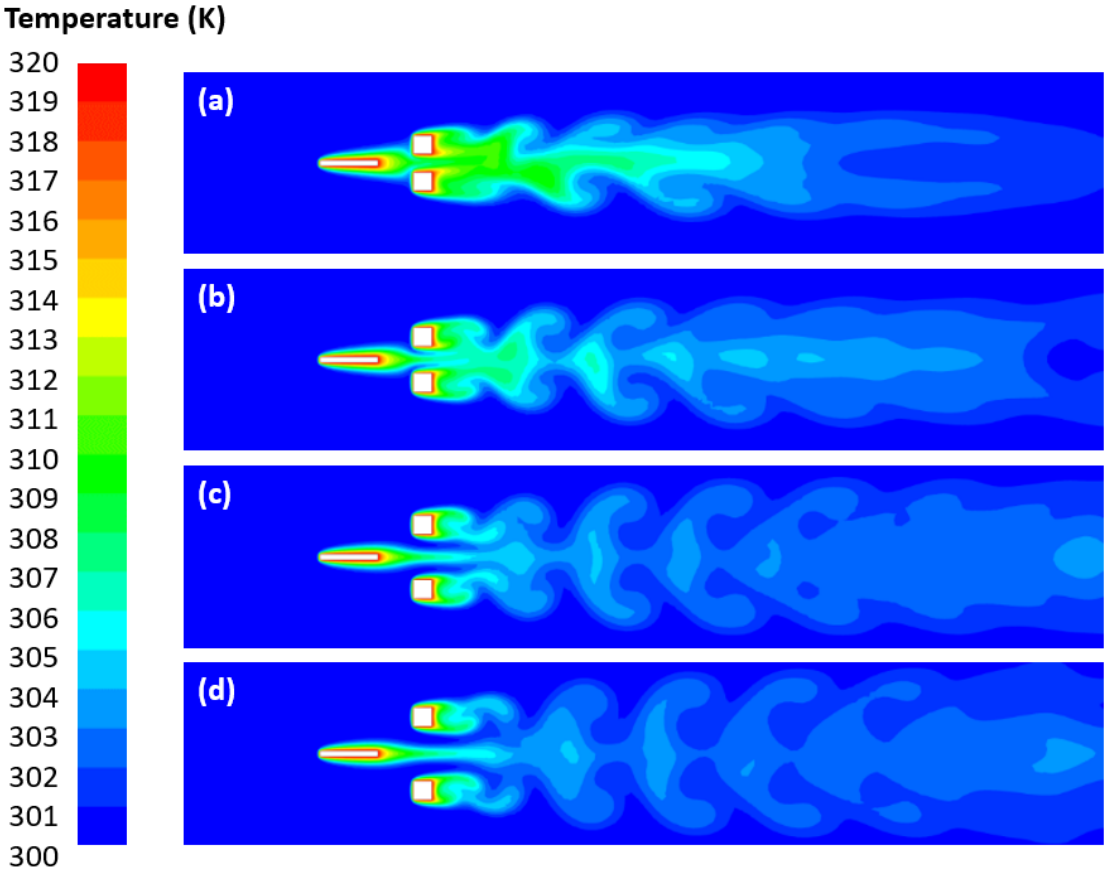


Figure 8 – Fields of temperature for $H_1/L_1$ = 0.1, $S_L/D$ = 4.0 and: (a) $S_T/D$ = 2.0, (b) $S_T/D$ = 2.5, (c) $S_T/D$ = 3.0 and (d) $S_T/D$ = 4.0.

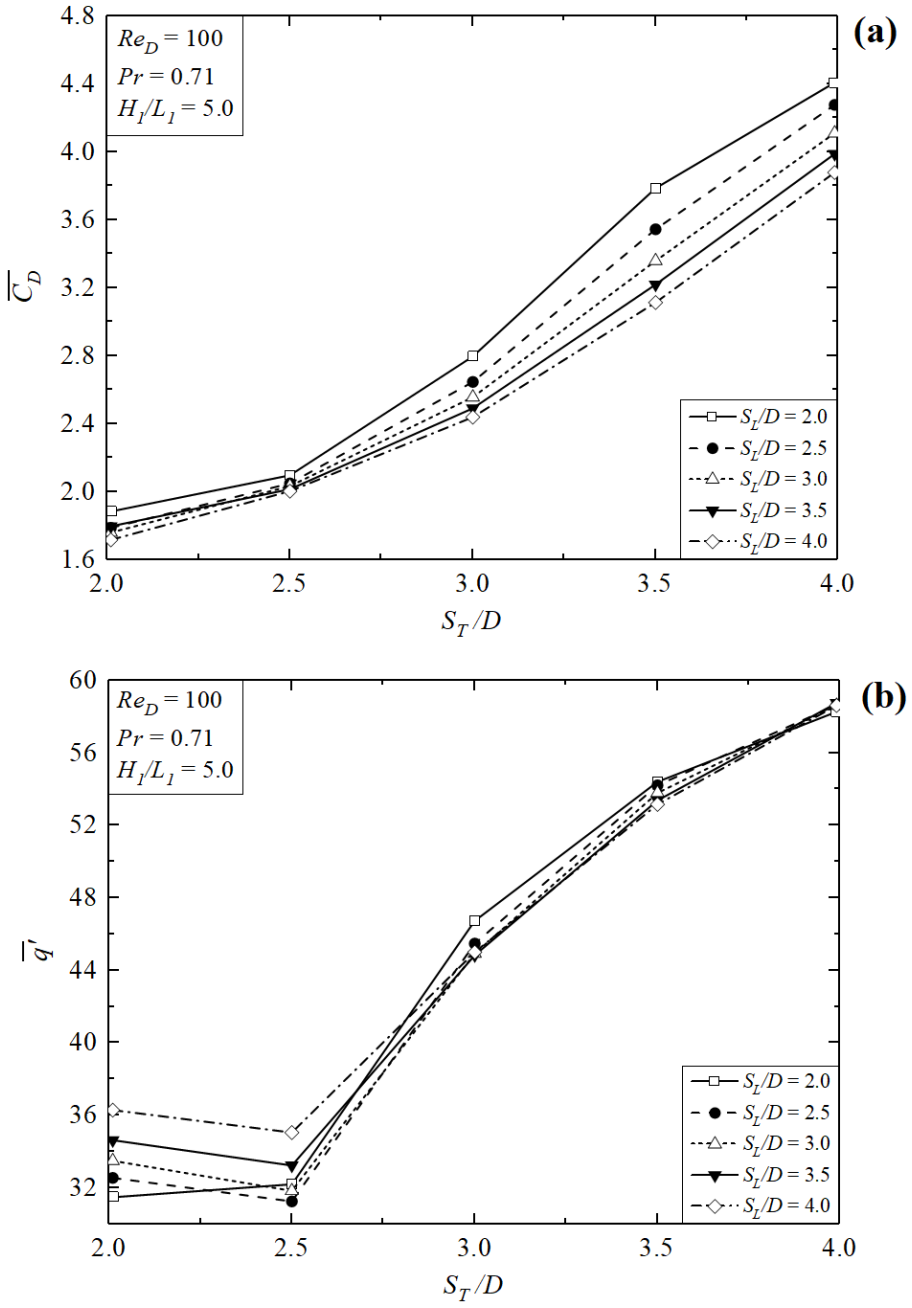


Figure 9 – Effect of $S_T/D$ over performance indicator for various values of $S_L/D$ and $H_1/L_1 = 5.0$: (a) drag coefficient and (b) heat transfer rate per unit length.

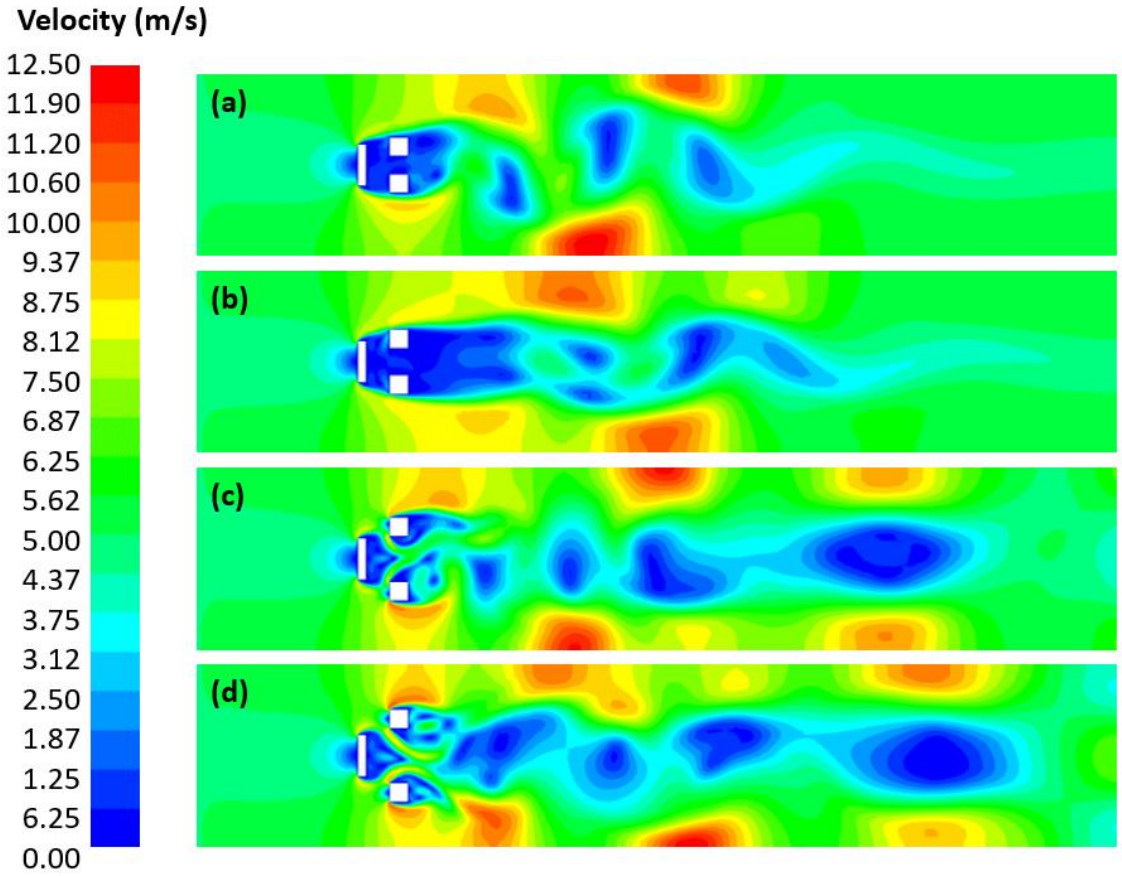


Figure 10 – Fields of velocity for $H_1/L_1$ = 5.0, $S_L/D$ = 2.0 and: (a) $S_T/D$ = 2.0, (b) $S_T/D$ = 2.5, (c) $S_T/D$ = 3.0 and (d) $S_T/D$ = 4.0.

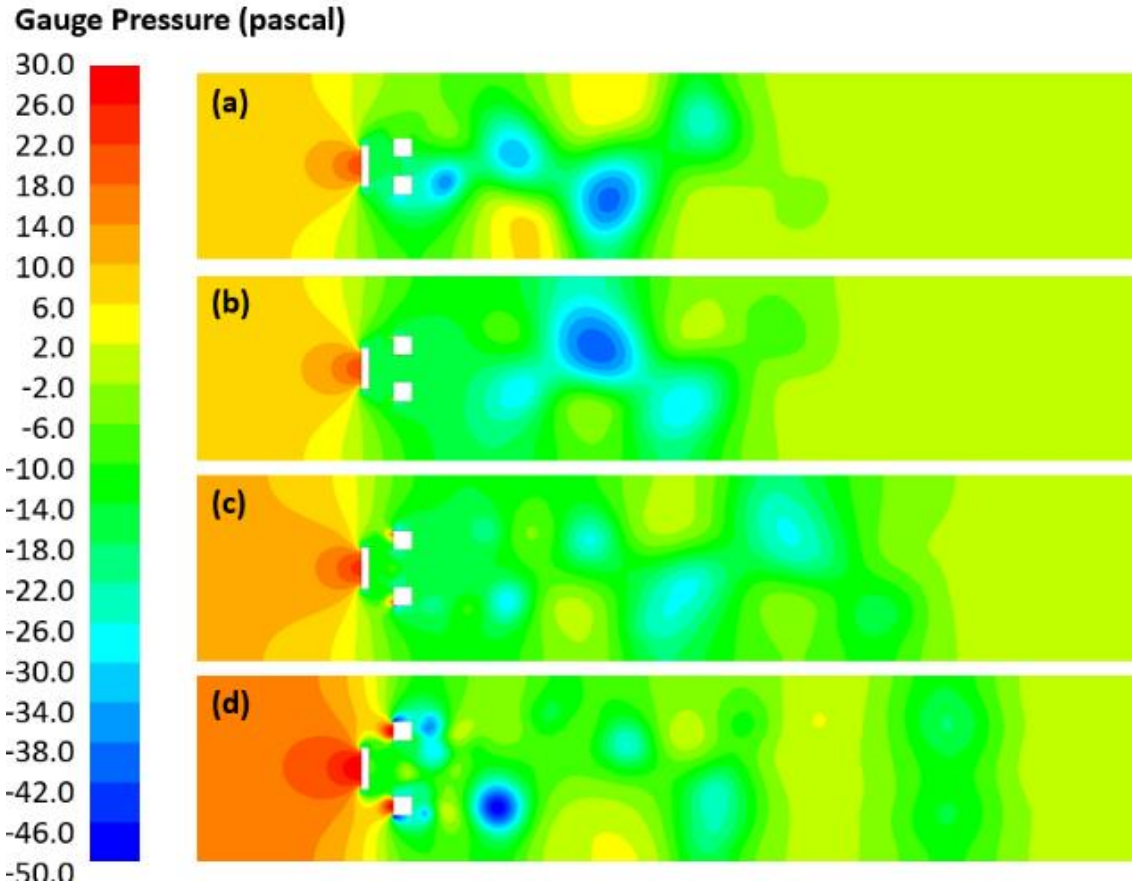


Figure 11 – Fields of pressure for $H_1/L_1$ = 5.0, $S_L/D$ = 2.0 and: (a) $S_T/D$ = 2.0, (b) $S_T/D$ = 2.5, (c) $S_T/D$ = 3.0 and (d) $S_T/D$ = 4.0.

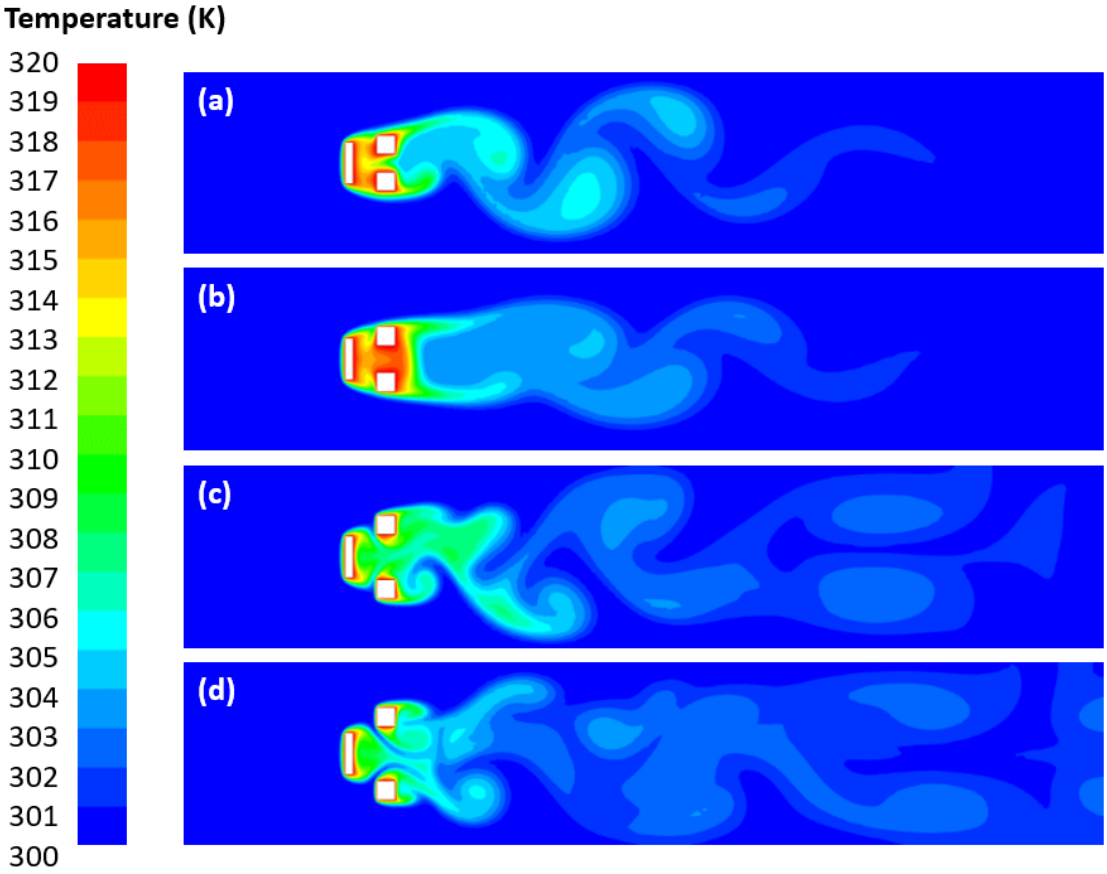


Figure 12 – Fields of temperature for $H_1/L_1$ = 5.0, $S_L/D$ = 2.0 and: (a) $S_T/D$ = 2.0, (b) $S_T/D$ = 2.5, (c) $S_T/D$ = 3.0 and (d) $S_T/D$ = 4.0.

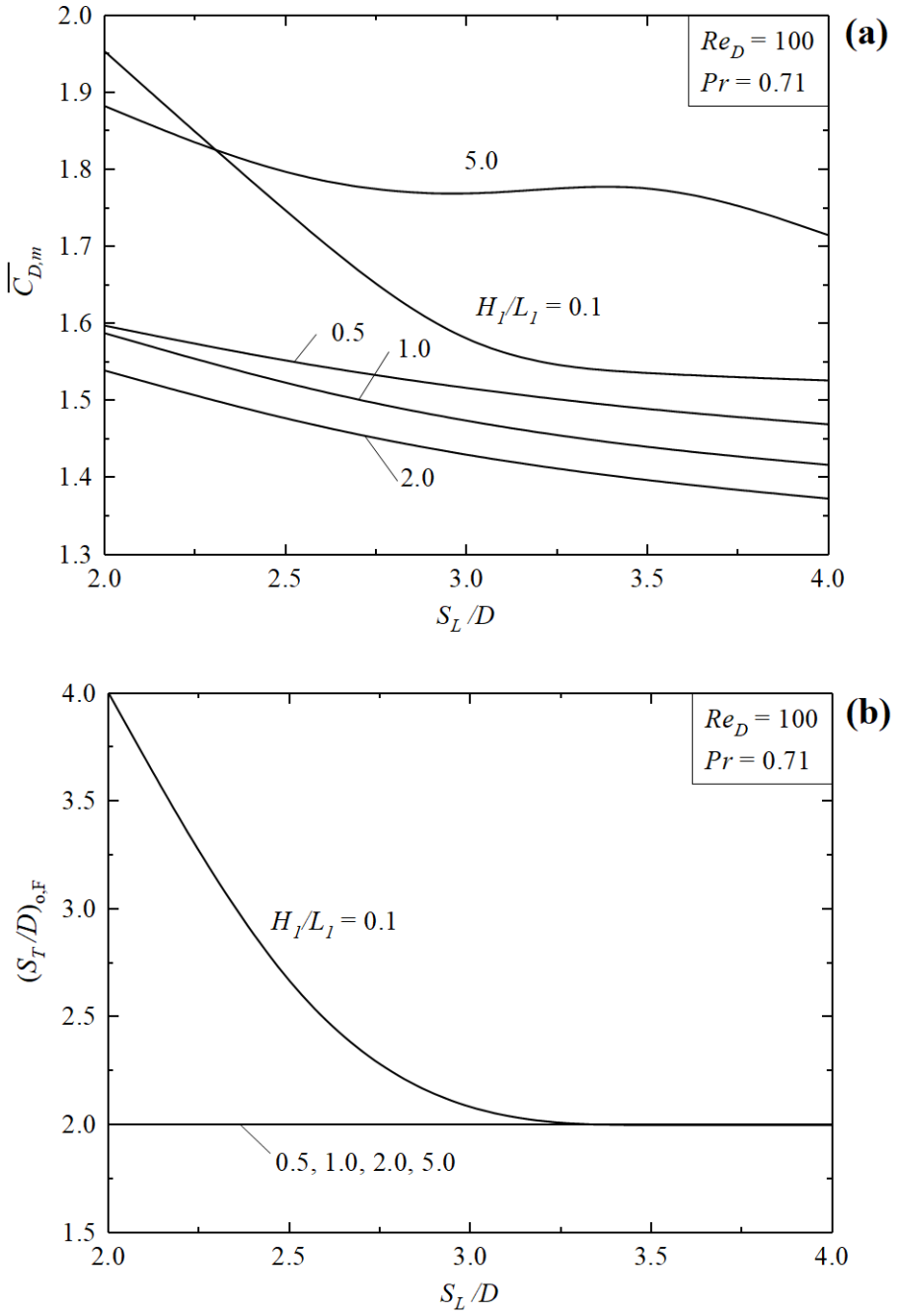


Figure 13 – Effect of $S_L/D$ over once minimized fluid dynamic performance indicator and corresponding optimal shape: a) $\overline{C_D}_{,m}$; b) $(S_T/D)_{o,F}$.

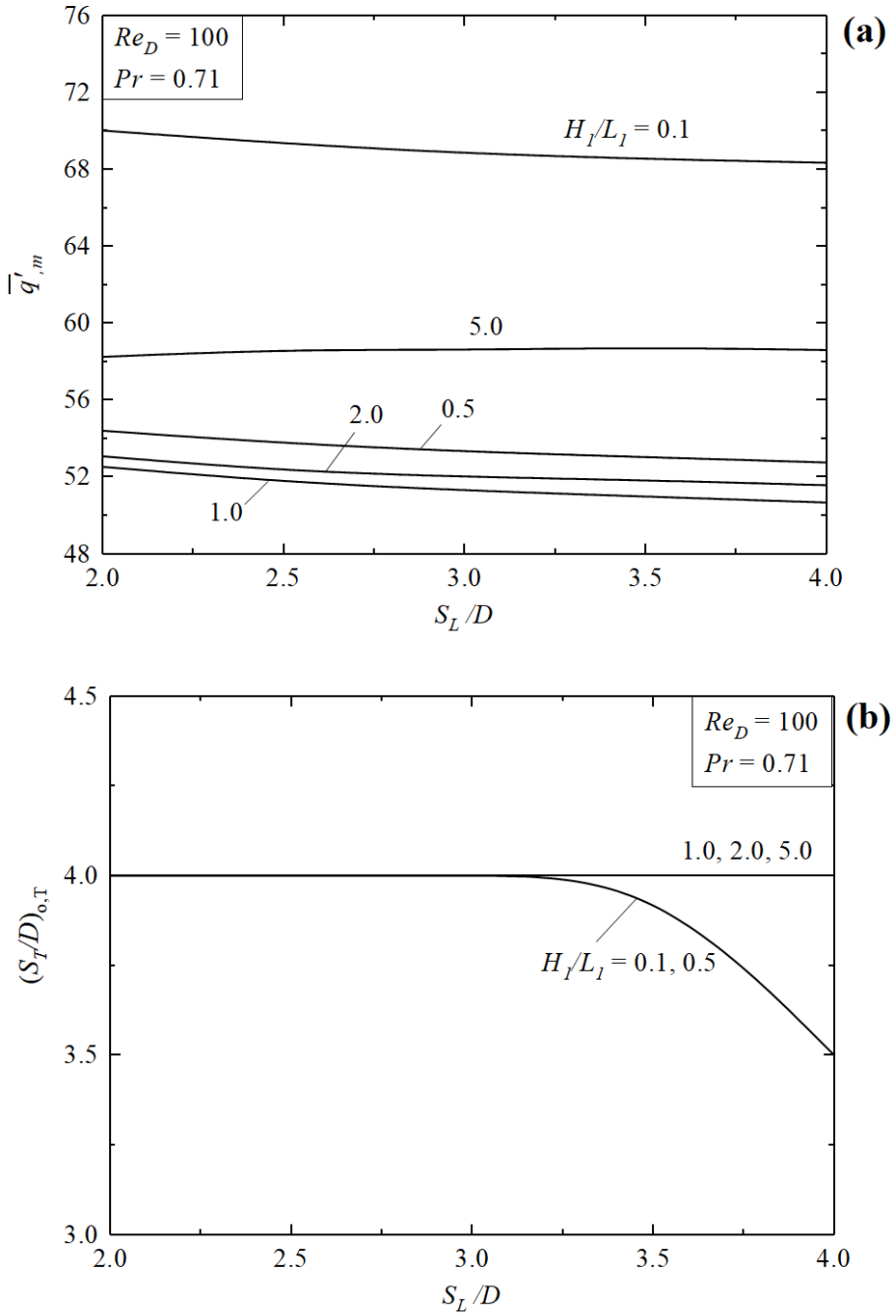


Figure 14 – Effect of $S_L/D$ over once maximized thermal performance indicator and corresponding optimal shape: a) $\overline{q}'_m$; b) $(S_T/D)_{o,T}$.

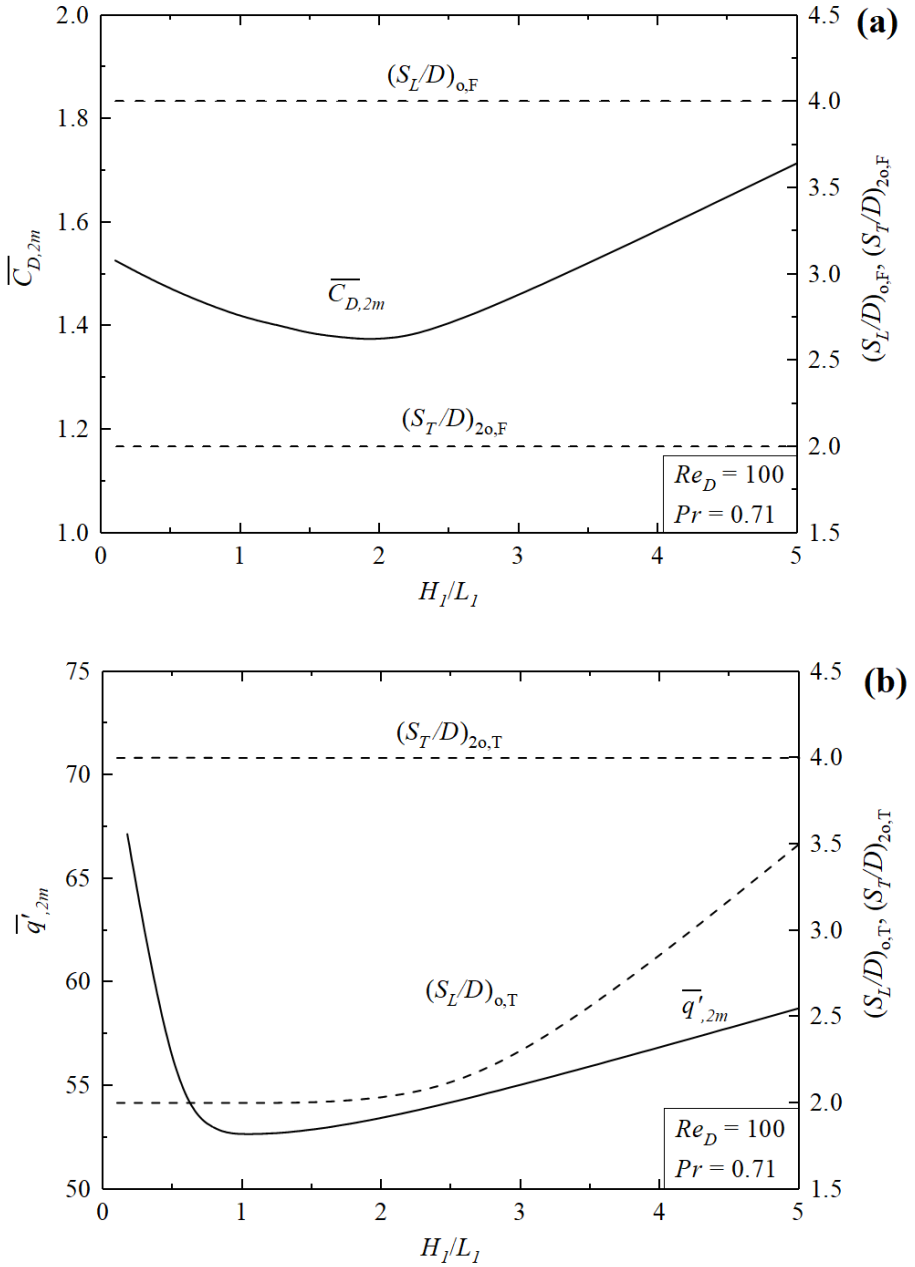


Figure 15 – Effect of $H_1/L_1$ over: a) $\overline{C_D}_{,2m}$, $(S_L/D)_{o,F}$ and $(S_T/D)_{2o,F}$; b) $\overline{q}'_{,2m}$, $(S_L/D)_{o,T}$ and $(S_T/D)_{2o,T}$.

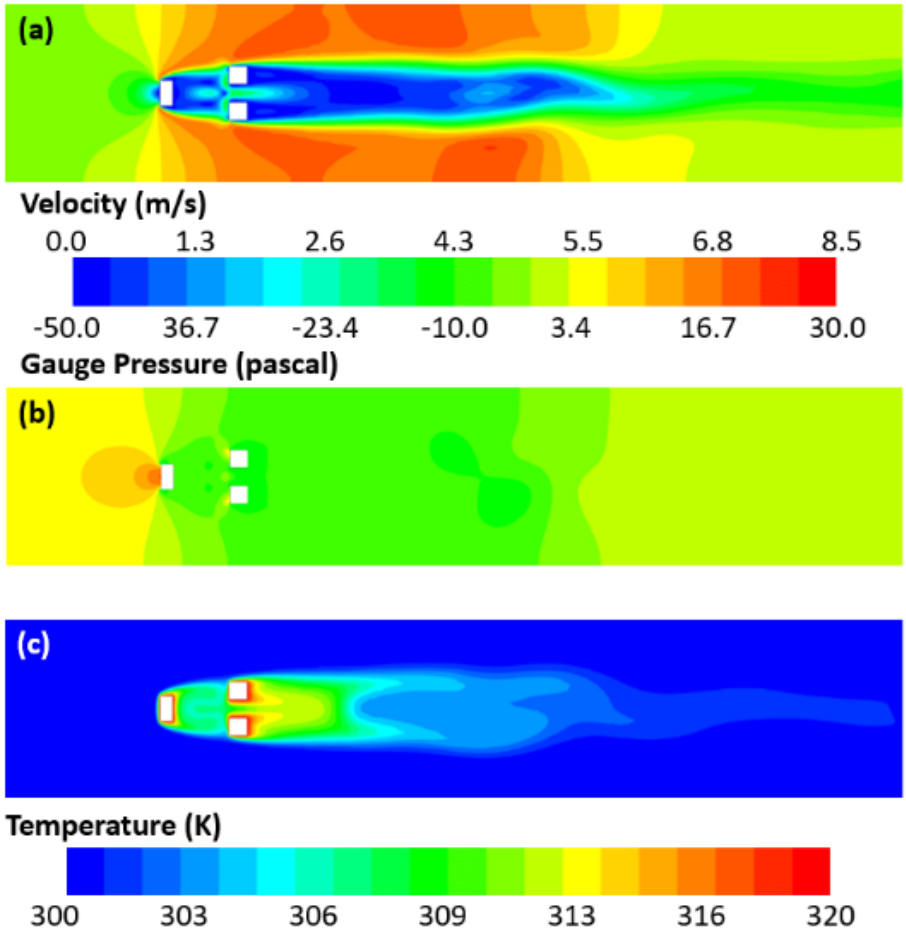


Figure 16 – Fields of (a) velocity, (b) pressure and (c) temperature, for the fluid dynamic optimum case ($\overline{C_D}_{,3m}$), $(H_1/L_1)_{o,F}$ = 2.0, $(S_L/D)_{2o,F}$ = 4.0 e $(S_T/D)_{3o,F}$ = 2.0.

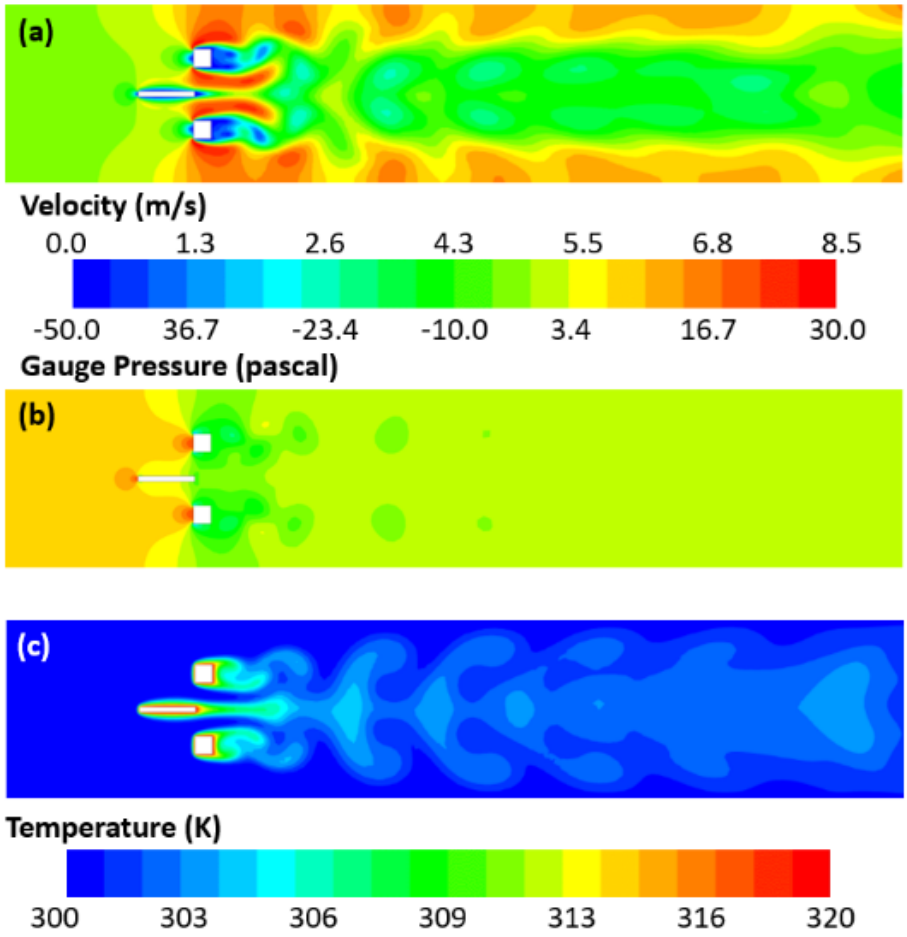


Figure 17 – Fields of (a) velocity, (b) pressure and (c) temperature, for the thermal optimum case ($\overline{q'}_{3m}$), $(H_1/L_1)_{o,T}$ = 0.1, $(S_L/D)_{2o,T}$ = 2.0 and $(S_T/D)_{3o,T}$ = 4.0.

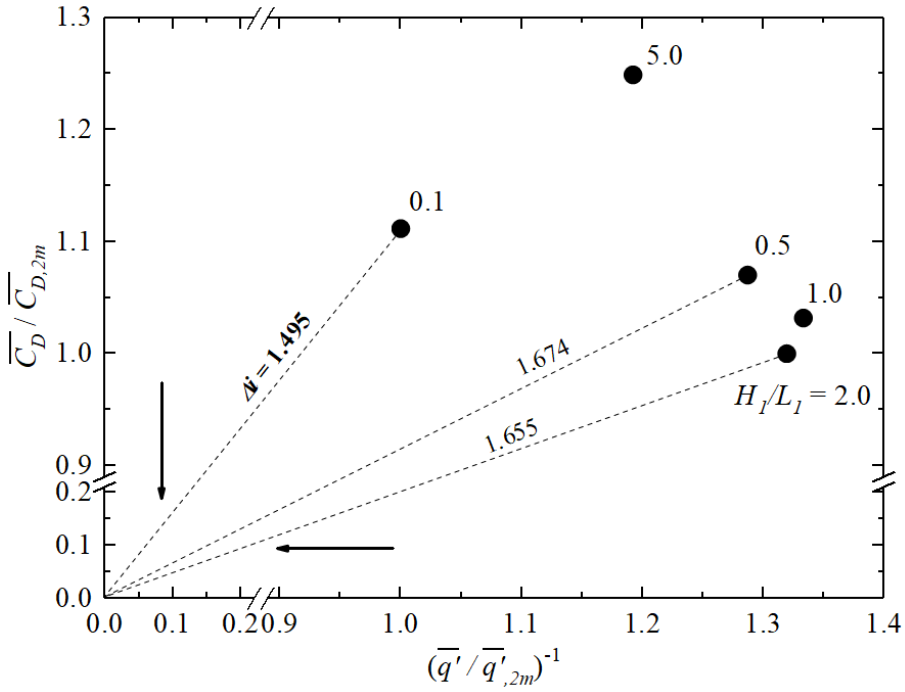


Figure 18 – Normalized values for twice minimized $\overline{C_D}$ versus the normalized inverse of twice maximized $\overline{q'}$ for various $S_L/D$.